References

1. Aoki K, Uchihara T, Tsuchiya K, Nakamura A, Ikeda K, Wakayama Y (2003) Enhanced expression of aquaporin 4 in human brain with infarction. Acta Neuropathol 106:121–124

2. Baló J (1928) Encephalitis periaxialis concentrica. Arch Neurol 19:242–263

3. Bennett JL, Lam C, Kalluri SR et al (2009) Intrathecal pathogenic anti-aquaporin-4 antibodies in early neuromyelitis optica. Ann Neurol 66:617–629

4. Bradl M, Misu T, Takahashi T et al (2009) Neuromyelitis optica: pathogenicity of patient immunoglobulin in vivo. Ann Neurol 66:630–643

5. Carmosino M, Procino G, Tamma G, Mannucci R, Svelto M, Valenti G (2007) Trafficking and phosphorylation dynamics of AQP4 in histamine-treated human gastric cells. Biol Cell 99:25–36

6. Chen CJ, Chu NS, Lu CS, Sung CY (1999) Serial magnetic resonance imaging in patients with Baló's concentric sclerosis: natural history of lesion development. Ann Neurol 46:651–656

7. Courville CB (1970) Concentric sclerosis. In: Vinken PJ, Bruyn GW (eds) Multiple sclerosis and other demyelinating diseases. North-Holland, Amsterdam, pp 437–451

8. Fenton RA, Moeller HB, Zelenina M, Snaebjornsson MT, Holen T, MacAulay N (2010) Differential water permeability and regulation of three aquaporin 4 isoforms. Cell Mol Life Sci 67:829–840

9. Frydenlund DS, Bhardwaj A, Otsuka T et al (2006) Temporary loss of perivascular aquaporin-4 in neocortex after transient middle cerebral artery occlusion in mice. Proc Natl Acad Sci USA 103:13532–13536

10. Fujita Y, Yamamoto N, Sobue K et al (2003) Effect of mild hypothermia on the expression of aquaporin family in cultured rat astrocytes under hypoxic condition. Neurosci Res 47:437–444

11. Graber JJ, Kister I, Geyer H, Khaund M, Herbert J (2010) Neuromyelitis optica and concentric rings of Baló in the brainstem. Arch Neurol 66:274–275

12. Jung JS, Bhat RV, Preston GM, Guggino WB, Baraban JM, Agre P (1994) Molecular characterization of an aquaporin cDNA from brain: candidate osmoreceptor and regulator of water balance. Proc Natl Acad Sci USA 91:13052–13056

13. Kinoshita M, Nakatsuji Y, Kimura T et al (2009) Neuromyelitis optica: passive transfer to rats by human immunoglobulin. Biochem Biophys Res Commun 386:623–627

14. Kinoshita M, Nakatsuji Y, Moriya M et al (2009) Astrocytic necrosis is induced by anti-aquaporin-4 antibody-positive serum. Neuroreport 20:508–512

15. Kuroiwa Y (1985) Neuromyelitis optica (Devic's disease, Devic's syndrome). In: Koetsier JC (ed) Handbook of clinical neurology. Demyelinating disease, vol 47. Elsevier, Amsterdam, pp 397–408

16. Lassmann H, Raine CS, Antel J, Prineas JW (1998) Immunopathology of multiple sclerosis: report on an international meeting held at the institute of neurology of the University of Vienna. J Neuroimmunol 86:213–217

17. Lee M, Lee SJ, Choi HJ et al (2008) Regulation of AQP4 protein expression in rat brain astrocytes: role of P2X7 receptor activation. Brain Res 1195:1–11

18. Lee TS, Eid T, Mane S et al (2004) Aquaporin-4 is increased in the sclerotic hippocampus in human temporal lobe epilepsy. Acta Neuropathol 108:493–502

19. Lennon VA, Kryzer TJ, Pittock SJ, Verkman AS, Hinson SR (2005) IgG marker of optic-spinal multiple sclerosis binds to the aquaporin-4 water channel. J Exp Med 202:473–477

20. Lennon VA, Wingerchuk DM, Kryzer TJ et al (2004) A serum autoantibody marker of neuromyelitis optica: distinction from multiple sclerosis. Lancet 364:2106–2112

21. Li L, Zhang H, Verkman AS (2009) Greatly attenuated experimental autoimmune encephalomyelitis in aquaporin-4 knockout mice. BMC Neurosci 10:94

22. Lucchinetti C, Brück W, Parisi J, Scheithauer B, Rodriguez M, Lassmann H (2000) Heterogeneity of multiple sclerosis lesions: implications for the pathogenesis of demyelination. Ann Neurol 47:707–717

23. Lucchinetti CF, Mandler RN, McGavern D et al (2002) A role for humoral mechanisms in the pathogenesis of Devic's neuromyelitis optica. Brain 125:1450–1461

24. Mahad D, Ziabreva I, Lassmann H, Turnbull D (2008) Mitochondrial defects in acute multiple sclerosis lesions. Brain 131:1722–1735

25. Manley GT, Fujimura M, Ma T, Noshita N, Filiz F, Bollen AW et al (2000) Aquaporin-4 deletion in mice reduces brain edema after acute water intoxication and ischemic stroke. Nat Med 6:159–163

26. Meng S, Qiao M, Lin L, Del Bigio MR, Tomanek B, Tuor UI (2004) Correspondence of AQP4 expression and hypoxic-ischaemic brain edema monitored by magnetic resonance imaging in the immature and juvenile rat. Eur J Neurosci 19:2261–2269

27. Misu T, Fujihara K, Kakita A et al (2007) Loss of aquaporin 4 in lesions of neuromyelitis optica: distinction from multiple sclerosis. Brain 130:1224–1234

28. Moeller HB, Fenton RA, Zeuthen T, Macaulay N (2009) Vasopressin-dependent short-term regulation of aquaporin 4 expressed in *Xenopus* oocytes. Neuroscience 164:1674–1684

29. Nag S, Manias JL, Stewart DJ (2009) Pathology and new players in the pathogenesis of brain edema. Acta Neuropathol 118:197–217

30. Roemer SF, Parisi JE, Lennon VA et al (2007) Pattern-specific loss of aquaporin-4 immunoreactivity distinguishes neuromyelitis optica from multiple sclerosis. Brain 130:1194–1205

31. Saadoun S, Waters P, Bell BA, Vincent A, Verkman AS, Papadopoulos MC (2010) Intra-cerebral injection of neuromyelitis optica immunoglobulin G and human complement produces neuromyelitis optica lesions in mice. Brain 133:349–361

32. Sabater L, Giralt A, Boronat A et al (2009) Cytotoxic effect of neuromyelitis optica antibody (NMO-IgG) to astrocytes: an in vitro study. J Neuroimmunol 215:31–35

33. Sharma R, Fischer MT, Bauer J et al (2010) Inflammation induced by innate immunity in the central nervous system leads to primary astrocyte dysfunction followed by demyelination. Acta Neuropathol 120:223–236

34. Stadelmann C, Ludwin S, Tabira T et al (2005) Tissue preconditioning may explain concentric lesions in Baló's type of multiple sclerosis. Brain 128:979–987

35. Verkman AS, Binder DK, Bloch O, Auguste K, Papadopoulos MC (2006) Three distinct roles of aquaporin-4 in brain function

revealed by knockout mice. Biochim Biophys Acta 1758:1085–1093

36. Vincent T, Saikali P, Cayrol R et al (2008) Functional consequences of neuromyelitis optica–IgG astrocyte interactions on blood–brain barrier permeability and granulocyte recruitment. J Immunol 181:5730–5737

37. Voskuhl RR, Peterson RS, Song B et al (2009) Reactive astrocytes form scar-like perivascular barriers to leukocytes during adaptive immune inflammation of the CNS. J Neurosci 29:11511–11522

38. Wang C, Zhang KN, Wu XM et al (2008) Baló's disease showing benign clinical course and co-existence with multiple sclerosis-like lesions in Chinese. Mult Scler 14:418–424

39. Wiendl H, Weissert T, Herrlinger U, Krapf H, Küker W (2005) Diffusion abnormality in Baló's concentric sclerosis: clues for the pathogenesis. Eur Neurol 53:42–44

40. Wolburg-Buchholz K, Mack AF, Steiner E, Pfeiffer F, Engelhardt B, Wolburg H (2009) Loss of astrocyte polarity marks blood–brain barrier impairment during experimental autoimmune encephalomyelitis. Acta Neuropathol 118:219–233

Contents lists available at ScienceDirect

Journal of the Neurological Sciences

journal homepage: www.elsevier.com/locate/jns
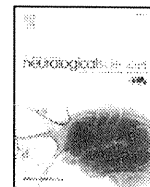
CSF angiotensin II and angiotensin-converting enzyme levels in anti-aquaporin-4 autoimmunity

T. Matsushita [a], N. Isobe [a], M. Kawajiri [b], M. Mogi [c], K. Tsukuda [c], M. Horiuchi [c], Y. Ohyagi [c], J. Kira [a,*]

[a] Department of Neurology, Neurological Institute, Graduate School of Medical Sciences, Kyushu University, Fukuoka, Japan
[b] Department of Neurology, Saiseikai Fukuoka General Hospital, Fukuoka, Japan
[c] Department of Molecular Cardiovascular Biology and Pharmacology, Ehime University, Graduate School of Medicine, Ehime, Japan

ARTICLE INFO

ABSTRACT

Background: Anti-aquaporin-4 (AQP4) antibody targets perivascular astrocyte foot processes, which contain abundant angiotensinogen, a precursor of angiotensin II, angiotensin-converting enzyme (ACE) and ACE2.
Objective: To disclose any abnormality in the intrathecal angiotensin II metabolic pathway in Japanese patients with neuromyelitis optica (NMO) or NMO spectrum disorders (NMOs) and positive for anti-AQP4 antibody.
Methods: We measured CSF angiotensin II, ACE and ACE2 levels in 15 anti-AQP4 antibody-positive patients with NMO or NMOs, 21 anti-AQP4 antibody-negative multiple sclerosis (MS) patients, 32 patients with other neurological diseases (OND) and 24 non-neurologic controls, using established ELISAs.
Results: CSF angiotensin II levels were lower in patients with NMO/NMOs (2.01 ± 1.82 pg/ml) and those with MS (3.15 ± 1.67 pg/ml) than in the OND (5.41 ± 2.34 pg/ml) and control groups (6.71 ± 2.65 pg/ml) ($P^{corr} < 0.005$). The difference in CSF angiotensin II levels between NMO/NMOs and MS patients was nearly significant ($P^{uncorr} = 0.052$). In NMO/NMOs and MS patients, angiotensin II levels were negatively correlated with CSF/serum albumin ratio ($P < 0.05$). ACE levels in CSF were lower in patients with NMO/NMOs (34.3 ± 5.61 ng/ml) than in MS patients (42.5 ± 8.19 ng/ml, $P^{corr} = 0.035$) and controls (44.7 ± 4.02 ng/ml, $P^{corr} < 0.0003$) while ACE2 levels were lower in NMO/NMOs (1.13 ± 0.49 ng/ml) and MS (1.75 ± 0.86 ng/ml) patients than in controls (2.76 ± 0.23 ng/ml, $P^{corr} < 0.001$ for both).
Conclusion: CSF angiotensin II, ACE, and ACE2 levels are decreased in NMO/NMOs patients with anti-AQP4 antibody, reflecting severe destruction of perivascular astrocytes.

1. Introduction

Angiotensin II is a potent vasoactive substance of the renin–angiotensin system (RAS), which plays an important role in regulating blood volume and systemic vascular resistance. Our previous work has demonstrated that angiotensin II attenuates brain damage and enhances neural differentiation via its receptor expressed on neuronal cells [1,2]. Moreover, we recently discovered reduced levels of angiotensin II in cerebrospinal fluid (CSF) from patients with multiple sclerosis (MS) [3], suggesting that the RAS may also be involved in the abnormal neural damage and repair processes in MS.

Angiotensin II is produced from its precursor, angiotensinogen; renin produces angiotensin I from angiotensinogen, and then angiotensin-converting enzyme (ACE) converts angiotensin I to angiotensin II [4]. Recently, a homologue of ACE, ACE2, was discovered; this enzyme cleaves angiotensin II to produce angiotensin-(1–7) (see Fig. 1 for the angiotensin

metabolic pathway) [4]. Perivascular astrocytes, a key constituent of the blood–brain barrier (BBB), abundantly express angiotensinogen, ACE and ACE2, and secrete angiotensin II in the CNS [5,6]. Secreted angiotensin II is supposed to up-regulate tight junction proteins in endothelial cells, which play a critical role in keeping the BBB tight [6]. In the chronic stage of MS, perivascular astrocytes are progressively lost [6], rendering the BBB leaky. The reduction of angiotensin II levels in the CSF that we observed may in part reflect such a process [3,7].

Neuromyelitis optica (NMO) is characterized by severe and selective involvement of the optic nerves and spinal cord. A specific IgG against NMO, designated NMO-IgG [8], targets aquaporin-4 (AQP4) on the perivascular astrocyte foot process [9]. We recently reported occurrences of extensive vasogenic edema in patients with anti-AQP4 antibody [10], possibly due to disruption of the AQP4 molecule regulating water flux in the CNS [11]. In Japanese patients with opticospinal MS (OSMS), some of whom also fulfill the proposed criteria for NMO, anti-AQP4 antibody is frequently detected [12,13]. These observations prompted us to study the levels of angiotensin II and its catalytic enzymes in the CSF of anti-AQP4 antibody-positive NMO patients, to uncover the relationship between the presence of anti-AQP4 antibody and BBB dysfunction.

* Corresponding author. Department of Neurology, Neurological Institute, Graduate School of Medical Sciences, Kyushu University, 311 Maidashi, Higashi-ku, Fukuoka 8128582, Japan. Tel.: +81 926425340; fax: +81 926425352.
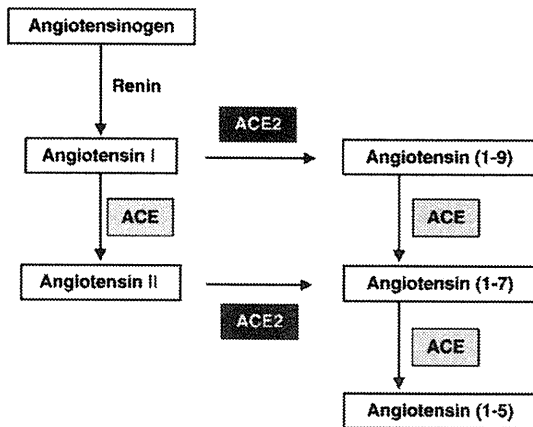E-mail address: kira@neuro.med.kyushuu.ac.jp (J. Kira).

Fig. 1. Schematic illustration of the metabolic pathway of the renin–angiotensin system. ACE = angiotensin-converting enzyme.

2. Materials and methods

2.1. Patients

Patients were examined in the Department of Neurology at Kyushu University Hospital and the Departments of Anesthesiology and Resuscitology at Ehime University Hospital, Japan between 2000 and 2008. Informed consent was obtained from each individual and the study protocol was approved by the ethics committees of both hospitals. We obtained CSF samples from 15 patients with anti-AQP4 antibody, the presence of which was determined by an immunofluorescence method using green fluorescence protein-AQP4 fusion protein-transfected human embryonic kidney cells, as described previously [12,13]. Among them, 12 patients fulfilled the revised NMO criteria [14] while three with myelitis or optic neuritis or both, who did not fully meet the criteria, were considered to have NMO spectrum disorders (NMOs). In addition, 21 MS patients who fulfilled the McDonald's MS criteria [15] and did not have anti-AQP4 antibody, 32 patients with other neurological diseases (OND) and 24 controls were also recruited (Table 1). The MS patients comprised 18 women and three men, while the 15 NMO/NMOs patients were all women. All MS and NMO/NMOs patients showed a relapsing–remitting course, and all CSF specimens were taken at relapse (within 30 days of the

Table 1
Demographic features of patients.

	NMO/NMOs	MS	OND
No. of patients	15	21	32
Men/women	0/15	3/18	25/7
Age at examination, years, mean ± SD	47.9 ± 12.7*	36.4 ± 12.5*	52.5 ± 16.4
Disease duration, years, mean ± SD	8.1 ± 5.3	8.0 ± 9.7	NA
Number of relapses, mean ± SD	9.7 ± 8.1	5.4 ± 3.9	NA
EDSS score, mean ± SD	5.7 ± 1.7*	3.9 ± 2.1*	NA
LESCLs during the entire course, n (%)	12 (80.0)*	6 (28.6)*	NA
CSF			
Cell count per μl, mean ± SD	9.1 ± 13.7	5.0 ± 6.6	1.5 ± 1.9
Total protein amount, mg/dl, mean ± SD	39.3 ± 19.1	33.5 ± 17.1	66.9 ± 38.7
CSF/serum albumin ratio, ×10⁴, mean ± SD	75.1 ± 38.9	53.6 ± 23.2	NA
IgG index, mean ± SD	0.56 ± 0.082*	0.74 ± 0.17*	NA
Oligoclonal IgG bands	0 (0.0)*	12 (57.1)*	NA

EDSS = Kurtzke's Expanded Disability Status Scale; LESCLs = longitudinally extensive spinal cord lesions; MS = multiple sclerosis; NMO = neuromyelitis optica; NMOs = neuromyelitis optica spectrum disorders; OND = other neurological diseases; NA = not applicable.
*P<0.05 in comparison between MS and NMO/NMOs patients. Percentages in parentheses.

initiation of relapse). Among the 21 MS patients, four received interferon β-1b (8 million units every other day) while two received low-to-medium doses of oral prednisolone (5.0 and 10 mg/day) at the time of lumbar puncture. Among the 15 patients with NMO/NMOs, four were treated with interferon β-1b and six were treated with chronic administration of oral prednisolone (2.5–40 mg/day) at the time of lumbar puncture. Among patients with MS and NMO/NMOs, the average ages at examination were 36.4 ± 12.5 (mean ± SD) and 47.9 ± 12.7 years, respectively, which were significantly different (P = 0.023). The average disease duration in these groups was 8.0 ± 9.7 and 8.1 ± 5.3 years, respectively (Table 1). Kurtzke's Expanded Disability Status Scale (EDSS) scores [16] (P = 0.0086) and the appearance rate of longitudinally extensive spinal cord lesions (LESCLs) extending over three or more vertebral segments during the entire course (P = 0.0059) were higher in NMO/NMOs patients than in MS patients. CSF total protein amount and CSF/serum albumin ratio were not different between patients with NMO/NMOs and those with MS (P>0.1), while the IgG index and the positivity rate for oligoclonal IgG bands were higher in MS patients than in NMO/NMOs patients (P = 0.015 and P = 0.0006, respectively). The OND group comprised 15 patients with chronic inflammatory demyelinating polyneuropathy (CIDP), nine with spinocerebellar degeneration and eight with Guillain–Barré syndrome. The control group of 24 patients (10 men and 14 women; age at examination: 45.3 ± 14.6 years) did not have any neurological or other diseases that might affect the angiotensin II levels in the CSF (18 patients underwent lumbar puncture during spinal anesthesia for operations for either urological or gynecological disorders; the other six cases underwent lumbar puncture because of suspected neurological diseases, but turned out to be neurologically normal). None of the patients or controls had hypertension, hypotension, or a metabolic disorder, and none took antihypertensive drugs. CSF samples were obtained by non-traumatic lumbar puncture and centrifuged within 30 min at 800 rpm at 4 °C for 5 min. The liquid phase of the CSF, which excluded sedimented cells, was stored at −80 °C until use.

2.2. Measurement of angiotensin II, ACE and ACE2 concentrations in the CSF

Angiotensin II, ACE and ACE2 concentrations in CSF were measured by established ELISA systems for angiotensin II (SPI-bio, Montigny-le-Bretonneux, France), ACE (R&D Systems, Minneapolis, MN), and ACE2 (AdipoGen Inc., Seoul, Korea), as described previously [3,7]. According to the manufacturer's data, the precision, recovery, and linearity of these assays are as follows: for the human angiotensin II ELISA, the intra-assay coefficients of variation (CVs) are 2.0–10.0%, inter-assay CVs are 5.0–15.0%, the recovery range is 80–115% and the linearity is around 90% of expected; for the human ACE ELISA, the intra-assay CVs are 3.4–4.0%, inter-assay CVs are 4.9–7.7%, the recovery range is 91–106% and linearity is around 105% of expected; for the human ACE2 ELISA, the intra-assay CVs are 5.3–9.9%, inter-assay CVs are 5.4–10.8%, the recovery range is 81–113%, and linearity is around 100% of expected.
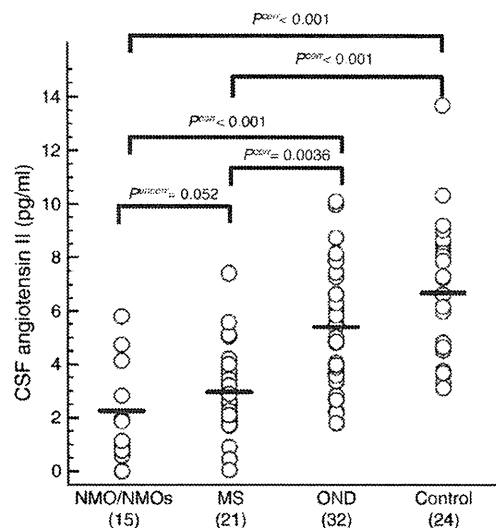
2.3. Statistical analysis

Statistical analyses of age at examination, disease duration, number of relapses, EDSS score, CSF cell count and total protein amount, CSF/serum albumin ratio, and IgG index between two subgroups were performed using the Mann–Whitney U-test. Comparisons of sex and numbers of LESCLs between two subgroups were performed using Fisher's exact probability test. Statistical analyses of angiotensin II, ACE and ACE2 levels were initially performed using the Kruskal–Wallis H-test. When differences were significant, the Mann–Whitney U-test was used to determine the significance of differences between groups. Uncorrected P values were corrected by multiplying them by the number of comparisons (Bonferroni–Dunn's correction)

Fig. 2. Angiotensin II levels in the CSF from patients with NMO/NMOs, MS, OND and controls. Bars indicate the mean concentration in each group. MS = multiple sclerosis; NMO = neuromyelitis optica; NMOs = neuromyelitis optica spectrum disorders; OND = other neurological diseases.

to calculate corrected P values (P^{corr}). Spearman's rank correlation test was used for statistical analyses of the correlations between angiotensin II levels in CSF and various clinical parameters. In all assays, significance was set at $P<0.05$.

3. Results

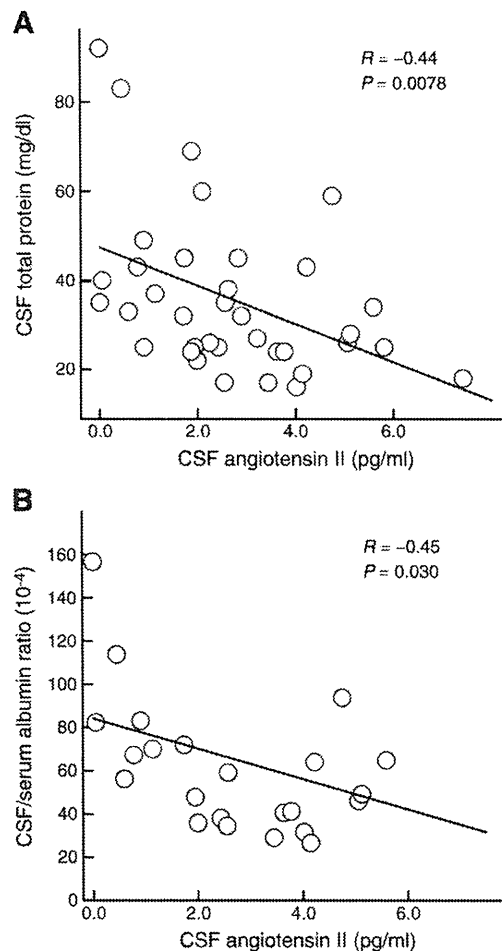### 3.1. Angiotensin II levels in the CSF

Angiotensin II levels in the CSF were 2.01 ± 1.82 pg/ml in the NMO/NMOs group, 3.15 ± 1.67 pg/ml in the MS group, 5.41 ± 2.34 pg/ml in the OND group and 6.71 ± 2.65 pg/ml in the control group (Fig. 2). The levels were significantly lower in the NMO/NMOs group and the MS group than in the OND group ($P^{corr} = 0.0036$ and $P^{corr}<0.001$) and the control group ($P^{corr}<0.001$ and $P^{corr}<0.001$). The difference in CSF angiotensin II levels between NMO/NMOs and MS patients was nearly significant ($P^{uncorr} = 0.052$). The level in the OND group was not different from that in the control group ($P^{corr}>0.1$). Exclusion of patients on prednisolone therapy gave practically the same results (data not shown). Among patients with MS or NMO/NMOs, there was no significant difference in angiotensin II levels between treated (prednisolone or interferon β-1b) and untreated patients ($P>0.1$).

3.2. Correlations between angiotensin II levels in the CSF and clinical parameters

Among patients with MS and NMO/NMOs, there were significant correlations of CSF angiotensin II levels with the CSF total protein amount ($R = -0.44$, $P=0.0078$) and CSF/serum albumin ratio ($R = -0.45$, $P=0.030$) (Fig. 3A, B). No significant correlations with clinical parameters, such as age at examination, disease duration, number of relapses, EDSS score, CSF cell count and IgG index, were noted in patients with NMO/NMOs.

3.3. ACE and ACE2 levels in the CSF

ACE levels in the CSF were 34.3 ± 5.61 ng/ml in NMO/NMOs patients, 42.5 ± 8.19 ng/ml in MS patients, and 44.7 ± 4.02 ng/ml in controls (Fig. 4A). The levels were significantly lower in NMO/NMOs patients than in MS patients ($P^{corr} = 0.035$) and controls ($P^{corr}<0.0003$), while they were not different between MS patients and controls ($P>0.1$). ACE2 levels

Fig. 3. (A) Correlation between angiotensin II levels and total protein amounts in the CSF in NMO/NMOs and MS patients. The number of patients represented is 36. (B) Correlations between CSF angiotensin II levels and the CSF/serum albumin ratio in NMO/NMOs and MS patients. The number of patients represented is 23.

in the CSF were 1.13 ± 0.49 ng/ml in NMO/NMOs patients, 1.75 ± 0.86 ng/ml in MS patients, and 2.76 ± 0.23 ng/ml in controls (Fig. 4B). The levels were significantly lower in patients with NMO/NMOs and MS than in controls ($P^{corr}<0.0003$ and $P^{corr} = 0.0006$, respectively), while they did not differ between NMO/NMOs and MS patients ($P>0.1$). Among patients with MS or NMO/NMOs, neither ACE nor ACE2 levels were different between treated (prednisolone or interferon β-1b) and untreated patients ($P>0.1$ and $P=0.097$, respectively).

4. Discussion

In this study, we uncovered severe reductions in angiotensin II, ACE and ACE2 levels in the CSF of NMO/NMOs patients. As an increase in CSF angiotensin II levels has been reported in patients with essential hypertension [17], we carefully excluded those with hypertension or on antihypertensive drugs. Moreover, we obtained essentially the same results even when removing those on corticosteroids. Therefore, we consider that the decrease in angiotensin II levels in the CSF of NMO/NMOs patients is not an artifact.

Angiotensin II levels became lower as the CSF/serum albumin ratio became higher, indicating that angiotensin II levels successively decrease as BBB breakdown becomes more severe. There was a more pronounced decrease in angiotensin II levels in NMO/NMOs patients, who were all positive for anti-AQP4 antibody in this study, than in MS patients, suggesting more severe BBB disruption in the former group.

A

B
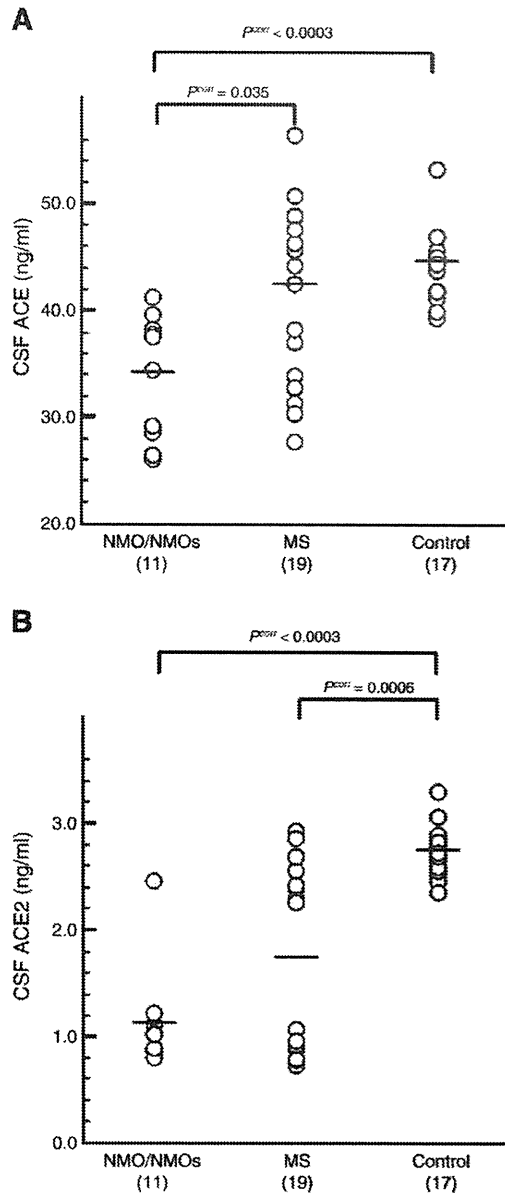
Fig. 4. ACE (A) and ACE2 (B) levels in the CSF from patients with NMO/NMOs and MS, and controls. Bars indicate the mean concentration in each group. ACE = angiotensin-converting enzyme; NMO = neuromyelitis optica; NMOs = neuromyelitis optica spectrum disorders.

We also found that both ACE and ACE2 levels were significantly decreased in NMO/NMOs patients. Because perivascular astrocytes are the main reservoirs of angiotensin II precursors and its metabolizing enzymes [5,6], the decrease in the levels of angiotensin II-metabolizing enzymes in NMO/NMOs patients' CSF suggests more severe destruction of astrocytes among anti-AQP4 antibody-positive patients than among MS patients without the antibody. Indeed, anti-AQP4 antibody, which mostly belongs to the IgG1 subclass [13], is supposed to disrupt astrocyte foot processes by fixing complements [18].

We previously reported an increase in the level of ACE and a decrease in the level of ACE2 in MS patients without anti-AQP4 antibody [7], and suggested a compensatory mechanism to be operative in response to a decrease in the level of angiotensin II, namely, up-regulation of the synthesizing enzyme (ACE) and down-regulation of the catabolizing enzyme (ACE2). Although we could not

reproduce the increase in ACE level in this series of MS patients, at least the ACE level was not decreased as compared with that in controls. It is possible that perivascular astrocyte destruction in MS is variable among cases, and sufficiently mild for the compensatory mechanism to work in some cases. Such a compensatory mechanism is no way operative in NMO/NMOs.

Wosik et al. [6] recently demonstrated that angiotensinogen knock-out mice had disorganized occludin strands at the level of the BBB, and that the numbers of perivascular astrocytes immunopositive for angiotensinogen were decreased in MS lesions; this decrease was correlated with reduced expression of the tight junction protein occludin. Angiotensin II is thus considered to up-regulate expression of this tight junction protein, which strengthens the BBB. Therefore, the reduction in the level of angiotensin II may in turn contribute to BBB dysfunction through the loss of its up-regulating effect on tight junction proteins in NMO/NMOs patients with anti-AQP4 antibody, who had a tendency for more frequent relapses than MS patients without the antibody [12]. Moreover, a recent study on experimental autoimmune encephalomyelitis using transgenic mice with targeted ablation of reactive astrocytes indicates that lack of perivascular astrocyte scar formation induces severe inflammation, further supporting a protective barrier function of perivascular astrocytes [19]. Grave disruption of perivascular astrocytes in NMO as suggested by the present study may well explain the frequent relapses and severe inflammation in this condition.

Angiotensin II binds two major receptors, angiotensin II type-1 (AT1) and -2 (AT2) receptors. Most of its actions on cardiovascular regulation and fluid balance are mediated by the AT1 receptor. This receptor is also expressed on T cells and macrophages, and angiotensin II induces a Th1 shift via stimulation of AT1 receptors [20]. As in NMO, Th2 cells are assumed to play a contributory role [21,22]: reduction of angiotensin II levels may enhance Th2 responses in NMO/NMOs patients, and thus, aggravate the illness. Angiotensin II also stimulates AT2 receptors expressed on the vascular wall and neuronal cells, and not only protects brain tissues from ischemia, but also enhances neural differentiation [1,2]. Therefore, the decrease in the levels of angiotensin II in NMO/NMOs patients' CSF may also indicate attenuated neuroprotection via the AT2 receptor. It is thus assumed that the marked reduction in the level of CSF angiotensin II in NMO/NMOs patients may result in detrimental effects on the disease process through BBB dysfunction, a Th2 shift, and attenuated neuroprotection.

Acknowledgements

References

[1] Mogi M, Li J-M, Iwanami J, Min L-J, Tsukuda K, Iwai M, et al. Angiotensin II type-2 receptor stimulation prevents neural damage by transcriptional activation of methyl methanesulfonate sensitive 2. Hypertension 2006;48:141–8.

[2] Li J-M, Mogi M, Tsukuda K, Tomochika H, Iwanami J, Min L-J, et al. Angiotensin II-induced neural differentiation via angiotensin II type 2 (AT2) receptor-MMS2 cascade involving interaction between AT2 receptor-interacting protein and Src homology 2 domain-containing protein-tyrosine phosphatase 1. Mol Endocrinol 2007;21:499–511.

[3] Kawajiri M, Mogi M, Osoegawa M, Matsuoka T, Tsukuda K, Kohara K, et al. Reduction of angiotensin II in the cerebrospinal fluid of patients with multiple sclerosis. Mult Scler 2008;14:557–60.

[4] Ferrario CM. Angiotensin-converting enzyme 2 and angiotensin-(1–7): an evolving story in cardiovascular regulation. Hypertension 2006;47:515–21.

[5] Gallagher PE, Chappell MC, Ferrario CM, Tallant EA. Distinct roles for ANG II and ANG-(1–7) in the regulation of angiotensin-converting enzyme 2 in rat astrocytes. Am J Physiol Cell Physiol 2006;290:C420–6.

[6] Wosik K, Cayrol R, Dodelet-Devillers A, Berthelet F, Bernard M, Moumdjian R, et al. Angiotensin II controls occludin function and is required for blood brain barrier maintenance: relevance to multiple sclerosis. J Neurosci 2007;27:9032–42.

[7] Kawajiri M, Mogi M, Higaki N, Matsuoka T, Ohyagi Y, Tsukuda K, et al. Angiotensin-converting enzyme (ACE) and ACE2 levels in the cerebrospinal fluid of patients with multiple sclerosis. Mult Scler 2009;15:262–5.

[8] Lennon VA, Wingerchuk DM, Kryzer TJ, Pittock SJ, Lucchinetti CF, Fujihara K, et al. A serum autoantibody marker of neuromyelitis optica: distinction from multiple sclerosis. Lancet 2004;364:2106–12.

[9] Lennon VA, Kryzer TJ, Pittock SJ, Verkman AS, Hinson SR. IgG marker of optic-spinal multiple sclerosis binds to the aquaporin-4 water channel. J Exp Med 2005;202: 473–7.

[10] Matsushita T, Isobe N, Matsuoka T, Ishizu T, Kawano Y, Yoshiura T, et al. Extensive vasogenic edema of anti-aquaporin-4 antibody-related brain lesions. Mult Scler 2009;15:1113–7.

[11] Tait MJ, Saadoun S, Bell BA, Papadopoulos MC. Water movements in the brain: role of aquaporins. Trends Neurosci 2008;31:37–43.

[12] Matsuoka T, Matsushita T, Kawano Y, Osoegawa M, Ochi H, Ishizu T, et al. Heterogeneity of aquaporin-4 autoimmunity and spinal cord lesions in multiple sclerosis in Japanese. Brain 2007;130:1206–23.

[13] Matsushita T, Isobe N, Matsuoka T, Shi N, Kawano Y, Wu X, et al. Aquaporin-4 autoimmune syndrome and anti-aquaporin-4 antibody-negative opticospinal multiple sclerosis in Japanese. Mult Scler 2009;15:834–47.

[14] Wingerchuk DM, Lennon VA, Pittock SJ, Lucchinetti CF, Weinshenker BG. Revised diagnostic criteria for neuromyelitis optica. Neurology 2006;66:1485–9.

[15] Polman CH, Reingold SC, Edan G, Filippi M, Hartung H-P, Kappos L, et al. Diagnostic criteria for multiple sclerosis: 2005 revisions to the "McDonald Criteria". Ann Neurol 2005;58:840–6.

[16] Kurtzke JF. Rating neurologic impairment in multiple sclerosis: an expanded disability status scale (EDSS). Neurology 1983;33:1444–52.

[17] Finkielman S, Fischer-Ferraro C, Diaz A, Goldstein DJ, Nahmod VE. A pressor substance in the cerebrospinal fluid of normotensive and hypertensive patients. Proc Natl Acad Sci USA 1972;69:3341–4.

[18] Jacob A, Matiello M, Wingerchuk DM, Lucchinetti CF, Pittock SJ, Weinshenker BG. Neuromyelitis optica: changing concepts. J Neuroimmunol 2007;187:126–38.

[19] Voskuhl RR, Peterson RS, Song B, Ao Y, Morales LBJ, Tiwari-Woodruff S, et al. Reactive astrocytes form scar-like perivascular barriers to leukocytes during adaptive immune inflammation of the CNS. J Neurosci 2009;29:11511–22.

[20] Shao J, Nangaku M, Miyata T, Inagi R, Yamada K, Kurokawa K, et al. Imbalance of T-cell subsets in angiotensin II-infused hypertensive rats with kidney injury. Hypertension 2003;42:31–8.

[21] Lucchinetti CF, Mandler RN, McGavern D, Bruck W, Gleich G, Ransohoff RM, et al. A role for humoral mechanisms in the pathogenesis of Devic's neuromyelitis optica. Brain 2002;125:1450–61.

[22] Ishizu T, Osoegawa M, Mei F-J, Kikuchi H, Tanaka M, Takakura Y, et al. Intrathecal activation of the IL-17/IL-8 axis in opticospinal multiple sclerosis. Brain 2005;128: 988–1002.

Contents lists available at ScienceDirect

NeuroImage

Oscillatory gamma synchronization binds the primary and secondary somatosensory areas in humans

Koichi Hagiwara [a,b,1], Tsuyoshi Okamoto [c,1], Hiroshi Shigeto [a,b,*], Katsuya Ogata [b], Yuko Somehara [b], Takuya Matsushita [a], Jun-ichi Kira [a], Shozo Tobimatsu [b]

[a] Department of Neurology, Neurological Institute, Graduate School of Medical Sciences, Kyushu University, Fukuoka, Japan
[b] Department of Clinical Neurophysiology, Neurological Institute, Graduate School of Medical Sciences, Kyushu University, Fukuoka, Japan
[c] Digital Organ, Digital Medicine Initiative, Kyushu University, Fukuoka, Japan

ARTICLE INFO

ABSTRACT

Induced gamma activity has a key role in the temporal binding of distributed cortico-cortical processing. To elucidate the neural synchronization in the early-stage somatosensory processing, we studied the functional connectivity between the primary and secondary somatosensory cortices (SI and SII) in healthy subjects using magnetoencephalography (MEG) with excellent spatiotemporal resolution. First, somatosensory-evoked magnetic fields were recorded to determine the locations of each cortical activity. Then we analyzed the phase-locking values (PLVs) of the induced gamma activity to assess neural synchrony within the somatosensory cortical network. We also assessed PLVs in patients with multiple sclerosis (MS) to validate our PLV analysis in evaluating the inter-areal functional connectivity, which can often be impaired in MS. The PLVs of the induced gamma activity were calculated for each pair of unaveraged MEG signals that represented the activities of the contralateral SI and bilateral SII areas. Analysis of PLVs between the SI and SII areas showed significantly increased PLVs for gamma-band activities, starting at an early post-stimulus stage in normal controls, whereas this increase in PLVs was apparently diminished in MS. The PLV analysis provided evidence for early-latency, gamma-band neuronal synchronization between the SI and SII areas in normal controls. Our study first demonstrates the gamma-band synchrony in the early-stage human somatosensory processing.

Introduction

In the somatosensory system, the primary and secondary somatosensory cortices (SI and SII) comprise the early stage of the hierarchical organization. Numerous neurophysiological studies have examined the functional differences between the two cortical areas in humans. Electrophysiological studies of evoked responses have often reported differences in activation timing between SI and SII (Pons et al., 1987; Mauguière et al., 1997; Inui et al., 2004), with the SI response occurring earlier than the SII responses. There are also studies with direct intracortical recording in epilepsy patients, which proved that SI and SII were activated in a sequential manner (Frot and Mauguière, 1999; Balzamo et al., 2004). The typical characteristics of SII include sensitivity towards higher order functions, such as sensorimotor integrations, attention, unitary body image, and integration of nociceptive and non-nociceptive information (for a

review, see Lin and Forss, 2002). Anatomically, it has been shown that the neurons in SII have larger and more complex receptive fields than those in SI (for a review, see Iwamura, 1998). Therefore, SII is often considered to be a hierarchically higher cortical area than SI.

Less is known about the functional connectivity between SI and SII in humans. Apart from the activation sequence of the cortical areas, few studies have evaluated functional connectivity between SI and SII in humans. Recently, it has become evident that neuronal synchronization plays an important role in distributed cortico-cortical processing: induced gamma activity could be related to the temporal binding of spatially distributed information processing in the mammalian brain (Tallon-Baudry and Bertrand, 1999; Engel and Singer, 2001; Buzsáki and Draguhn, 2004; Knight, 2007). To date, however, whether the temporal binding mechanism with the gamma-band activity relates to the somatosensory processing between SI and SII has not been demonstrated. To clarify this issue, we applied magnetoencephalography (MEG) to evaluate neural synchrony in the gamma-band during the median nerve stimulation in healthy subjects. We analyzed phase-locking values (PLVs) of induced gamma activity between the somatosensory cortices. To validate our PLV analysis in evaluating functional connectivity between the distributed cortical areas, we also assessed PLVs in patients with

* Corresponding author. Department of Clinical Neurophysiology, Neurological Institute, Graduate School of Medical Sciences, Kyushu University, 3-1-1 Maidashi, Higashi-ku, Fukuoka 812-8582, Japan. Fax: +81 92 642 5352.
E-mail address: shigetou@neuro.med.kyushu-u.ac.jp (H. Shigeto).
[1] These authors contributed equally to this work.

clinically definite multiple sclerosis (MS). MS is known to cause multiple disconnections between distributed regions of the brain owing to demyelination and axonal loss in the central nervous system (Calabrese and Penner, 2007; Dineen et al., 2009; He et al., 2009). Here we provide evidence for early-stage, gamma-band neuronal synchronization between SI and SII for somatosensory information processing in humans.

Methods

Subjects

Twenty-three healthy volunteers (18 women and 5 men, mean age 37.3 ± 10.6 years) and 23 patients with clinically definite MS (18 women and 5 men, mean age 38.8 ± 8.1 years) according to the revised McDonald criteria (Polman et al., 2005) participated in this study. With respect to the MS patients, the mean duration of disease was 10.0 ± 7.3 years, and the mean Kurtzke Expanded Disability Status Scale Score (Kurtzke, 1983) was 2.7 ± 2.7. The clinical courses of the patients were relapsing–remitting in 17 patients, secondary progressive in four patients, and primary progressive in two patients. All the patients showed only mild disability and were ambulatory. On the basis of clinical histories obtained during routine follow-up, clinically evident sensory symptoms were documented in the right arm in 10 patients, and in the left arm, in nine patients. Somatosensory-evoked potentials were measured in 19 patients, and either delayed central conduction time or an absent N20 response was observed in four patients in response to right median nerve stimulation and seven patients in response to left median nerve stimulation. Nineteen patients showed typical brain lesions fulfilling the Barkhof magnetic resonance imaging (MRI) criteria (Barkhof et al., 1997): nine T2 hyperintense lesions present in nineteen patients, at least one infratentorial lesion present in seventeen patients, at least one juxtacortical lesion present in seventeen patients, at least three periventricular lesions present in twenty-two patients. In most patients, their clinical manifestations were usually caused by lesions in the optic nerves, brainstem, cerebellum, and spinal cord. No patients showed cognitive decline. None of the patients had anti-aquaporin-4 antibody, as confirmed by immunofluorescence technique (Matsuoka et al., 2007). Four patients were examined during a relapse period. This study was approved by the local ethics committees of our university, and written consent was obtained from all subjects.

Stimuli

Left and right median nerves were stimulated at the wrist in a separate recording with constant current pulses of 0.2-ms duration. The stimulus intensity was adjusted above the motor threshold to produce slight contraction of the abductor pollicis brevis muscle. At this intensity, large myelinated fibers but not small ones were stimulated. The stimuli were given pseudo-randomly, and the inter-stimulus interval ranged from 2.5 to 3.5 s (mean interval: 3 s) to avoid habituation of SII responses.

Data acquisition and processing

The MEG signals were acquired using a whole-head 306-channel sensor array (Vectorview, ELEKTA Neuromag, Helsinki) that comprises 102 identical triple-sensor elements. Each sensor element consists of two orthogonal planar-type gradiometers and one magnetometer. In this study, we analyzed MEG data recorded by the 204-channel planar-type gradiometers (gradiometers reduce external artifact signals, including geomagnetic signals and other environmental artifact signals). Prior to the recording, four head

position indicator (HPI) coils were attached to the scalp, and a 3D digitizer was used to measure anatomical landmarks of the head with respect to the HPI coils. During the recording, subjects lay on a bed in a magnetically shielded room with their heads positioned inside the helmet-shaped sensor array. The precise location of the head with respect to the sensor array was determined using the HPI coils. The recording bandpass filter was 0.03–1500 Hz, and the sampling rate was 5 kHz. The subjects were instructed to keep their eyes open and not to sleep; their vigilance levels were monitored by spontaneous MEG signals over the parieto-occipital areas and a video camera positioned in a shielded room. During the stimulation, we only stored raw data for off-line analysis. A spatiotemporal signal space separation (tSSS) method was applied off-line to the recorded raw data. tSSS is a software method that removes artifact signals arising from outside the sensor helmet (Taulu and Simola, 2006), and thus, theoretically, only artifact-free raw data were stored for further analysis.

Data analysis

Analysis of somatosensory-evoked magnetic fields (SEFs)

First, we analyzed conventional SEFs to determine the sensors representing activities of SI and SII. Off-line averaging of SEFs was performed using the tSSS-reconstructed raw data in the following condition: the analysis epoch was 50 ms before and 250 ms after the stimulus, and 100–120 responses were averaged for each median nerve. The averaged responses were digitally bandpass filtered in the 0.3–150 Hz range with a notch filter of 60 Hz. The prestimulus period from −50 ms to −10 ms was used as a baseline. The peak latencies and amplitudes of SEF waveforms were determined by root–mean–square (RMS) waveforms reconstructed from the two orthogonal gradiometers to better identify the sensors showing the maximal responses (Kida et al., 2006). We analyzed evoked responses generated by three sources: the SI area in the hemisphere contralateral to the median nerve stimulation (cSI) and the bilateral secondary somatosensory areas (cSII and iSII, for contralateral and ipsilateral SII areas, respectively). For responses in cSI, three deflections (i.e., N20m, P35m, and P60m) were recorded. For each of the five deflections (N20m, P35m, P60m, cSII, and iSII), we searched for the sensor with the maximum amplitude, and peak latencies were determined at the time point showing the maximal amplitude. In the somatosensory paradigm used in this study, several cortical areas other than SI and SII could be activated such as the posterior parietal cortex and the mesial cortex of the paracentral lobule (Forss et al., 1994, 1996; Mauguière et al., 1997). Here, we focused on SI and SII responses to elucidate the functional interaction of these somatosensory cortices.

Equivalent current dipoles (ECDs) that explained the most dominant sources of each deflection were calculated by a least-squares fit using approximately 30 channels around the sensor with the maximum response. For analysis of the bilateral SII responses, the ECD of the P35m deflection (if P35m was not apparent, then P60m) was subtracted from the original waveforms using the signal space projection (SSP) method to remove the magnetic fields of cSI, because the isocontour fields of cSII could be hidden by those of cSI. The ECD analysis yielded the three-dimensional locations and strengths of the ECDs in a spherical conductor model. Because MRI was performed only in four subjects from the control group, the centers of the individual head coordinate system were standardized using the center of device coordinate ($x = 0$ mm, $y = 0$ mm, $z = 40$ mm) in both groups. Only the ECDs with goodness-of-fit values exceeding 80% were accepted for statistical analyses.

The peak latencies and amplitudes of the RMS waveforms were examined by Mann–Whitney U-test. The correlation between the latencies of cSI and bilateral SII responses was assessed by calculating Pearson's correlation coefficient. A Chi-square test was used to compare the numbers of evoked deflections between normal subjects and MS

patients. A probability level of 0.05 or less was considered to represent a significant difference throughout the statistical examinations.

Phase-locking analysis of gamma-band cortical activity

To evaluate the neuronal synchronization between the SI and SII areas, we calculated the PLVs of the stimulus-related gamma-band activity (Lachaux et al., 1999). First, to analyze oscillatory gamma-band activity, a continuous wavelet transform was applied to the tSSS reconstructed raw data. A temporal-frequency response is given by the temporal convolution of an MEG signal with the wavelet centering at center frequency f_0 and time t:

$$\Phi_k^m(t, f_0) = \int_{-\infty}^{\infty} s_k^m(\tau) \Psi_{f_0}^*(\tau - t) d\tau$$

where $s_k^m(\tau)$ represents the signal of kth trial recorded by channel m. In this transformation, we used a complex Morlet wavelet:

$$\Psi_{f_0}(\tau) = \frac{1}{\sqrt{\omega_0}} exp\left(-\frac{\tau^2}{2\sigma^2}\right) exp(i\omega_0\tau)$$

where $\omega_0 = 2\pi f_0$, $\omega_0\sigma = 7$. The wavelet analysis yielded induced gamma-band activities. Epochs for the wavelet transformation ranged from −250 to 350 ms relative to the stimulus onset. Second, we selected a sensor with maximal RMS amplitude of N20m deflection as a sensor representing cSI activity, and sensors with maximal RMS amplitudes of cSII and iSII responses were determined as sensors
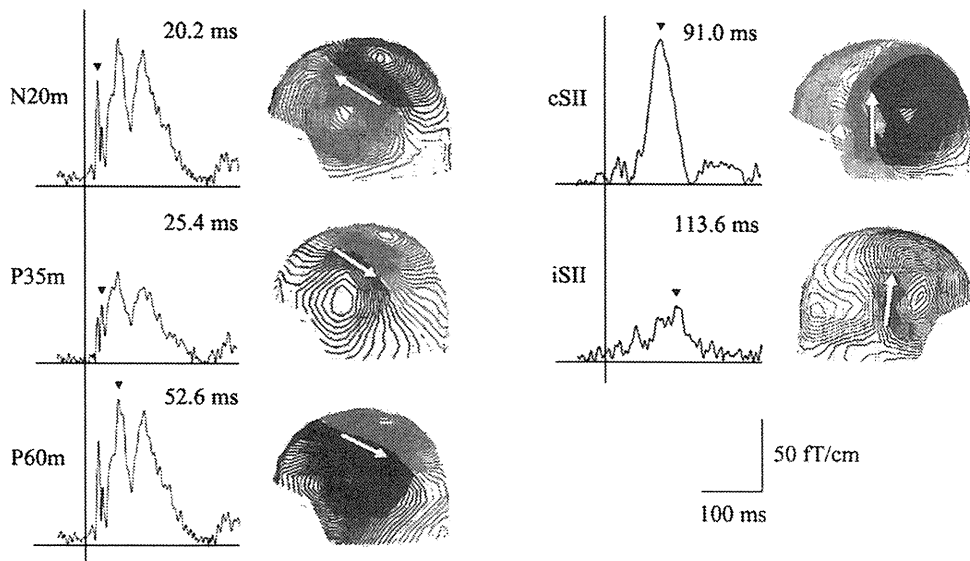
Normal subject

(A) Original waveforms
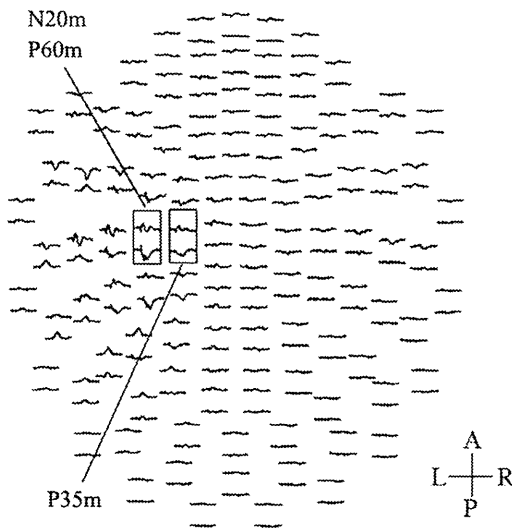
(B) After applying SSP
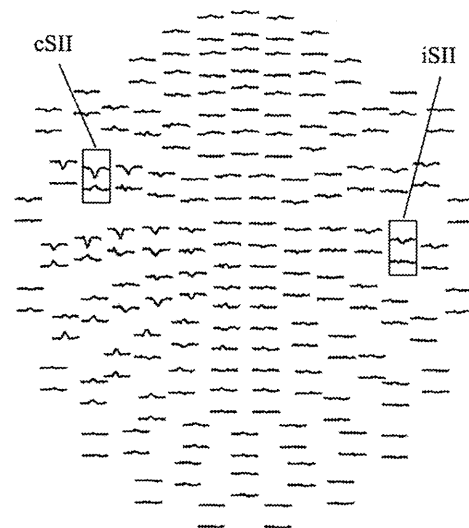
(C) RMS waveforms and isocontour maps

Fig. 1. Analysis of SEFs in a representative normal subject. (A) Original SEF waveforms are averaged from the tSSS reconstructed signals. (B) After subtracting the P35m response from the original waveforms by the SSP method, the sensors show only bilateral SII responses. (C) RMS waveforms at sensors with maximal peak amplitude of each deflection and corresponding field distributions (isocontour maps). The red lines indicate outgoing magnetic signals, while the blue lines ingoing magnetic signals. The arrows denote the current direction of the corresponding ECDs.

representing bilateral SII activities. PLV between two channels was calculated as follows:

$$PLV^{m,n}(t,f_0) = \left| \frac{1}{N} \sum_{k=1}^{N} \frac{\Phi_k^m(t,f_0)}{|\Phi_k^m(t,f_0)|} \Big/ \frac{\Phi_k^n(t,f_0)}{|\Phi_k^n(t,f_0)|} \right|$$

where m and n denote channels comprising the reference sensor and target sensor, respectively. PLV was calculated for each single trial, and the PLVs of 100 trials were averaged in each subject. PLVs are shown as an index ranging from 0 to 1.

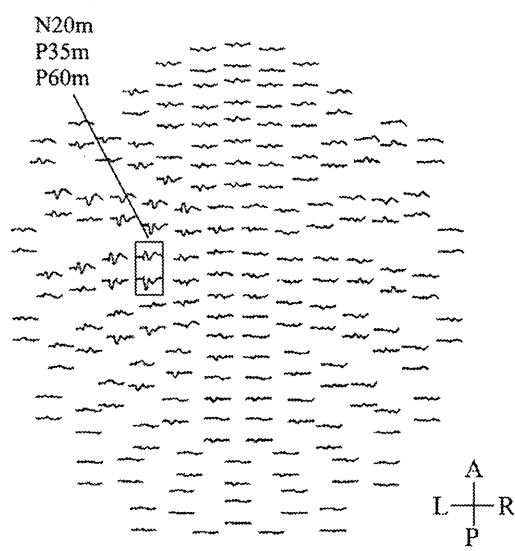Third, we examined phase-locking statistics (PLS) to determine whether the calculated PLVs were significantly correlated with the stimuli. PLS was defined by the proportion of surrogate PLVs higher than the original PLVs. The surrogate PLV represents the PLV calculated between signals of different trials:

$$PLV^{m,n}_{surrogate}(t,f_0) = \left| \frac{1}{100} \sum_{k=1}^{100} \frac{\Phi_{perm,k}^m(t,f_0)}{|\Phi_{perm,k}^m(t,f_0)|} \Big/ \frac{\Phi_k^n(t,f_0)}{|\Phi_k^n(t,f_0)|} \right|$$
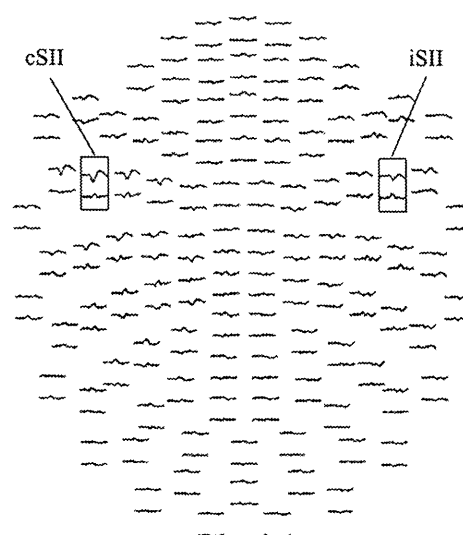
Here, we calculated the surrogate PLVs from 200 different permutations of trials. The statistically significant PLV was defined as the presence of surrogated PLVs of less than 10 trials larger than original PLVs (that is, PLS < 0.05). Furthermore, the mean PLV of the pre-stimulus period (−100 to 0 ms) was subtracted from the PLV of the
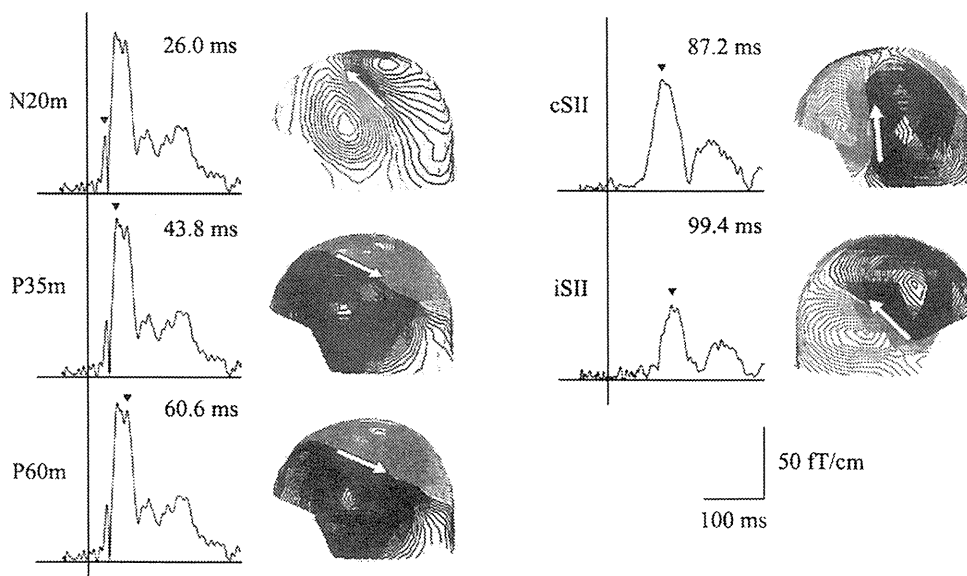
MS patient

(A) Original waveforms

N20m
P35m
P60m

A
L —— R
P

(B) After applying SSP

cSII   iSII

(C) RMS waveforms and isocontour maps

N20m   26.0 ms

P35m   43.8 ms

P60m   60.6 ms

cSII   87.2 ms

iSII   99.4 ms

50 fT/cm

100 ms

Fig. 2. Analysis of SEFs in an MS patient. The latencies of all cSI deflections (namely, N20m, P35m, and P60m) are prolonged compared with those in the normal subjects, whereas bilateral SII responses are evoked with comparable latencies. The amplitude of the N20m deflection is decreased, but other deflections, including the bilateral SII, are comparable in the amplitude to those in normal subjects.

Table 1
Latencies and amplitudes (mean ± SD) of the RMS waveforms.

	Latency (ms)			Amplitude (fT/cm)		
	Normal	MS	p value	Normal	MS	p value
N20m	21.4 ± 1.0 (n = 46)	23.5 ± 3.8 (n = 45)	0.027*	64.9 ± 30.1	52.1 ± 25.9	0.018*
P35m	32.0 ± 5.0 (n = 46)	35.6 ± 6.5 (n = 40)	0.005*	75.3 ± 48.7	74.3 ± 39.1	0.616
P60m	53.8 ± 7.6 (n = 46)	57.8 ± 8.4 (n = 46)	0.01*	90.2 ± 31.3	88.2 ± 47.4	0.281
cSII	91.2 ± 15.8 (n = 46)	87.2 ± 14.9 (n = 46)	0.153	60.8 ± 23.4	65.0 ± 33.6	0.656
iSII	104.2 ± 19.8 (n = 44)	104.1 ± 22.9 (n = 41)	0.728	41.4 ± 18.0	41.9 ± 18.6	0.778

* $P < 0.05$: when compared with the values in normal subjects using the Mann–Whitney U-test.

post-stimulus period; thus, only event-related phase synchronization of gamma-band activities was evaluated.

For the analysis of the group average, we selected regions of interest (ROIs) as follows: the frequency range was 30–70 Hz, and the latency period was 0–200 ms. PLVs were calculated for each orthogonally oriented pair of channels to minimize crosstalk noise, and the mean PLV was calculated from the ROI in each subject. Only PLVs with larger means were accepted for the group-averaged PLV ($p < 0.05$ by Rayleigh test).

Results

SEFs of SI and SII

In line with the results of previous studies (Kakigi, 1994; Wikström et al., 1996; Lin and Forss, 2002; Huttunen et al., 2006), we recorded five major deflections of the SEF waveforms in the cSI and bilateral SII areas. Figs. 1 and 2 show the representative SEF waveforms and isocontour maps obtained from normal subjects and MS patients. Short-latency deflections, N20m, P35m, and P60m, which corresponded to the activities of the cSI area, were identified over the contralateral centro-parietal area. Middle-latency deflections were observed over the bilateral temporo-parietal area with the deflection

contralateral to the stimulation peaking earlier than the deflection ipsilateral to the stimulation: the former corresponds to the activity of cSII, while the latter corresponds to the activity of iSII. All cSI deflections were clearly identified in all normal subjects, whereas N20m and P35m deflections were not recorded in one hemisphere ($p = 0.31$) and six hemispheres ($p < 0.01$), respectively, in MS patients. The cSII deflection was identified in all normal subjects as well as in all MS patients. The iSII deflection was undetectable in two hemispheres in normal subjects and in five hemispheres in MS patients ($p = 0.22$).

Regarding the side-to-side difference within each group, there were no significant differences in the peak latencies or in the amplitudes between the left and right median nerves. Therefore, the data for left and right median nerve stimulations were combined for the statistical analysis. Table 1 shows the latencies and amplitudes of the RMS waveforms. The mean latencies of all of the cSI deflections were significantly prolonged in MS patients ($p < 0.05$). By contrast, there were no significant differences in the latencies of bilateral SII deflections. In both groups, cSII and iSII were recorded at around 90 and 100 ms after stimulation, respectively. The mean amplitudes of the N20m deflection were significantly smaller in MS patients ($p < 0.05$). The amplitudes of other deflections showed no significant differences between MS and normal subjects. No significant correlation was found between the latencies for N20m and cSII in both
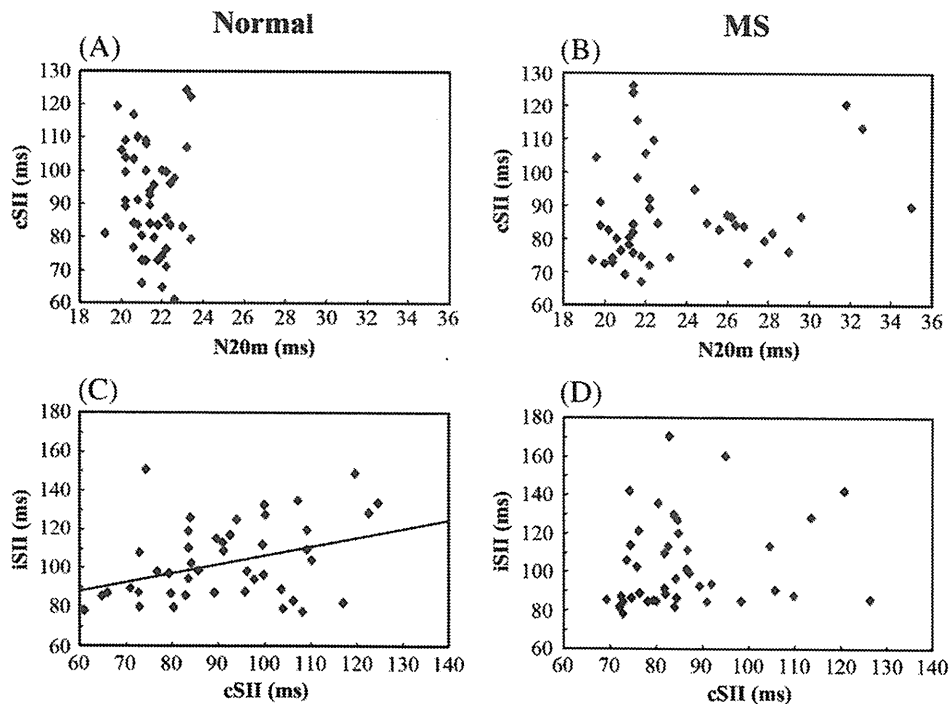
Fig. 3. A linear regression analysis of correlation between the latencies of cSI and cSII shows no significant correlation both in normal subjects (A; $r = 0.09$, $p = 0.55$) and MS patients (B; $r = 0.18$, $p = 0.23$). Correlation analysis between the latencies of cSII and iSII shows a significant correlation in normal subjects (C; $r = 0.361$, $p = 0.016$) but not in MS patients (D; $r = 0.158$, $p = 0.323$).

groups (Fig. 3A and B). There was a significant correlation between the latencies of cSII and iSII in normal subjects ($p < 0.05$) (Fig. 3C), but no correlation was found in MS patients (Fig. 3D). The mean locations and strengths of the ECDs for each deflection were almost comparable with those reported previously (see Supplemental data) (Wikström et al., 1996; Wegner et al., 2000; Kida et al., 2006). Fig. 4 shows the locations of the ECDs superimposed on the MRI in representative subjects of both groups, demonstrating that the ECDs are located in the appropriate cortices (i.e., SI and SII).

PLVs between SI and SII

The temporal-frequency analysis with the continuous wavelet transformation showed the induced gamma-band activities both in the SI and SII areas (Figs. 5 and 6). They started at early post-stimulus period and continued up to 200 ms. In normal subjects, high-frequency gamma activities (50–70 Hz) were observed in cSI, and to a lesser degree in cSII. Low-frequency gamma activities (30–40 Hz) were distributed in all three areas (i.e., cSI, cSII, and iSII). Interestingly, the power of the high-frequency gamma activities (50–70 Hz) was relatively reduced in MS patients. Figs. 7 and 8 show the grand averaged PLVs in the gamma-band (30–70 Hz) for the normal subjects and MS patients. Overall, PLVs were calculated in the range of 0–0.15. In normal subjects, significantly increased PLVs between cSI and cSII were observed mostly within the time window 0–100 ms after the stimulus onset (Fig. 7A). Increased PLVs in the higher frequency gamma-band (50–70 Hz) were observed within the early period (0–

50 ms) following the stimulus onset, whereas high PLVs in the lower frequency gamma-band (30–40 Hz) tended to last for a longer period, up to 100 ms. In addition, there were some weak but statistically significant PLVs of various frequency bands in the later time window 100–200 ms. On the contrary, the cSI–cSII phase synchrony was significantly decreased in MS patients, both in the high-frequency gamma-band (50–70 Hz) and the low-frequency gamma-band (30–40 Hz) (Fig. 7B). The degree of decrease in the PLVs between cSI and cSII was most prominent around 40 Hz. Regarding the phase synchrony between the cSII and iSII areas, significantly increased PLVs in the low-frequency gamma-band (30–40 Hz) were observed during the time interval 30–100 ms in normal subjects (Fig. 8A), whereas such an increase in PLVs was diminished in MS patients (Fig. 8B).

Discussion

Neuronal synchronization in the gamma-frequency band has received increasing attention as the salient mechanism for cortico-cortical information processing (Tallon-Baudry and Bertrand, 1999; Engel and Singer, 2001; Buzsáki and Draguhn, 2004; Knight, 2007; Womelsdorf et al., 2007). Recently, the temporal binding mechanism in various gamma-frequency bands has been well recognized in several studies of top–down and bottom–up information processing among anatomically distributed cortical areas (Tallon-Baudry et al., 1997; Engel et al., 2001; Womelsdorf et al., 2006; Buschman and Miller, 2007; Saalmann et al., 2007). However, the significance of temporal binding theory in the functional relationship between SI and SII has not yet been established. In this study, we assessed the temporal binding mechanism by PLVs of induced gamma activity, and our results provided evidence for functional interaction in the early somatosensory processing. To our knowledge, we first demonstrated that synchronized gamma-band activities in both between cSI and cSII and between cSII and iSII occurred in the early post-stimulus stage. Therefore, the oscillatory gamma synchronization binds the early-stage tactile information processing within the somatosensory cortical network.

Previous studies demonstrated that broadband oscillatory activities including the gamma-frequency bands were present and enhanced in relation to the attentive task in the early-stage somatosensory processing areas (Palva et al., 2005; Bauer et al., 2006). Until recently, no studies have examined the gamma-band phase synchronization between the SI and SII areas. Only cSI–iSII phase-locking in the alpha- and beta-frequency bands has been demonstrated in healthy subjects (Simões et al., 2003). Therefore, our study is the first to demonstrate the early-latency neural synchrony within the gamma-band between SI and SII, which may well represent the parallel mode of the early-stage tactile somatosensory processing. Although we did not perform attentive task to enhance the oscillatory gamma activity, the increase in PLVs after the stimulus onset (see Fig. 7) may be associated with ongoing cortical activities facilitating the later stages of somatosensory processing and perceptual process (Palva et al., 2005).

It is well known that SII receives direct thalamocortical projections from several nuclei of the thalamus, including the ventroposterior lateral nucleus, the ventroposterior inferior nucleus, the ventroposterior medial nucleus, the central lateral nucleus, and the posterior nucleus (Friedman and Murray, 1986; Krubitzer and Kaas, 1992; Stevens et al., 1993). In a study that applied a cortical cooling procedure in marmoset monkeys (Zhang et al., 1996, 2001), evoked responses and responsiveness of individual neurons in SII were rarely abolished by inactivation of SI, and the study claimed that SI and SII occupied a hierarchically equivalent position in the somatosensory system. In humans, simultaneous activation of SI and SII was suggested by an MEG study (Karhu and Tesche, 1999), which demonstrated very early evoked responses of SII; the initial activity

(A) **(B)**
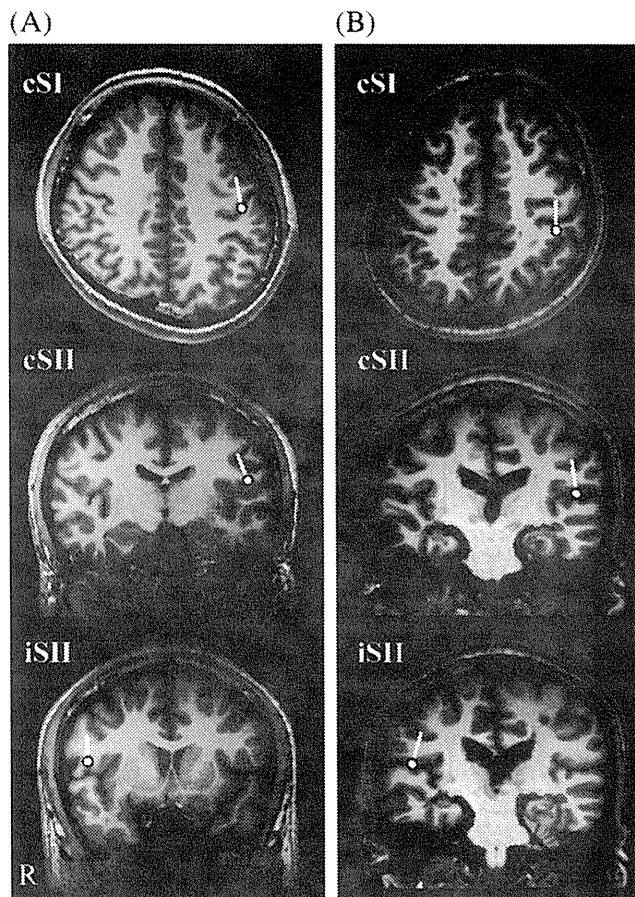
Fig. 4. ECD locations in a normal subject (A) and an MS patient (B) superimposed on MRI. For this view, cSI (N20m) and bilateral SII sources are located in the appropriate cortices in both subjects. The MS patient has scattered small hypointensities in the periventricular and juxtacortical white matter.
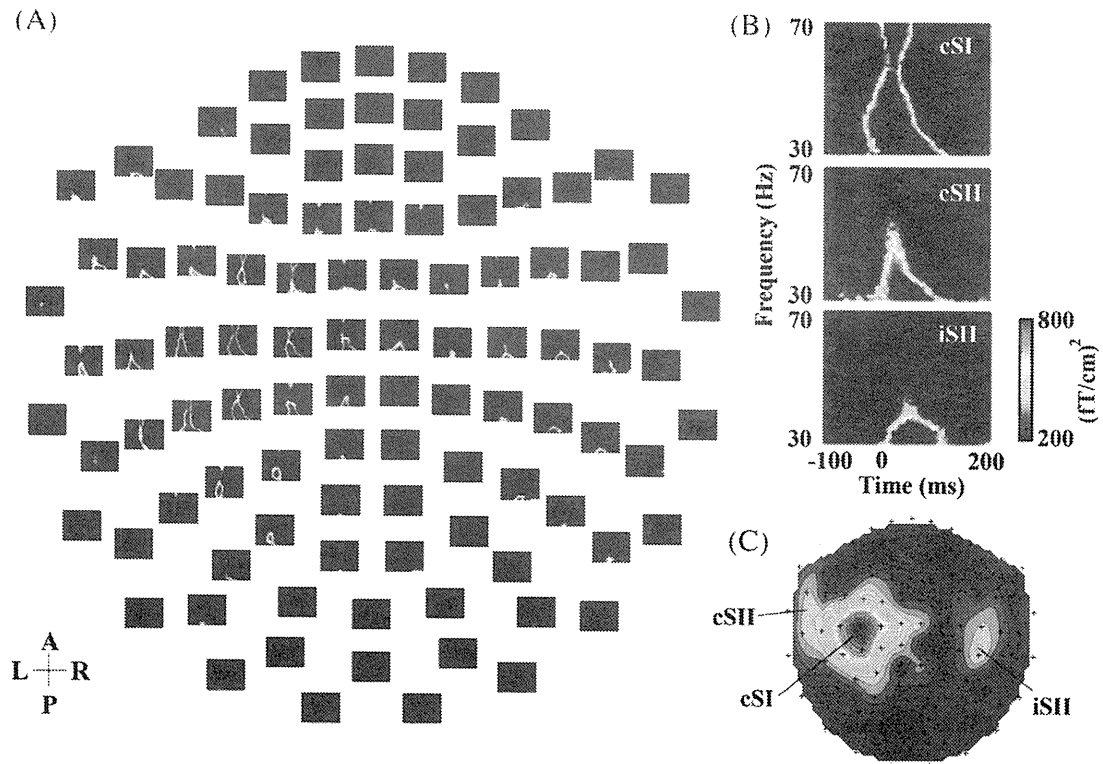
Fig. 5. (A) Temporal-frequency analysis for all gradiometer sensors in a representative normal subject. (B) Induced gamma-band activities (30–70 Hz) recorded by the sensors showing the SI and SII activities. (C) Topography of the induced gamma activities around the SI and SII areas.
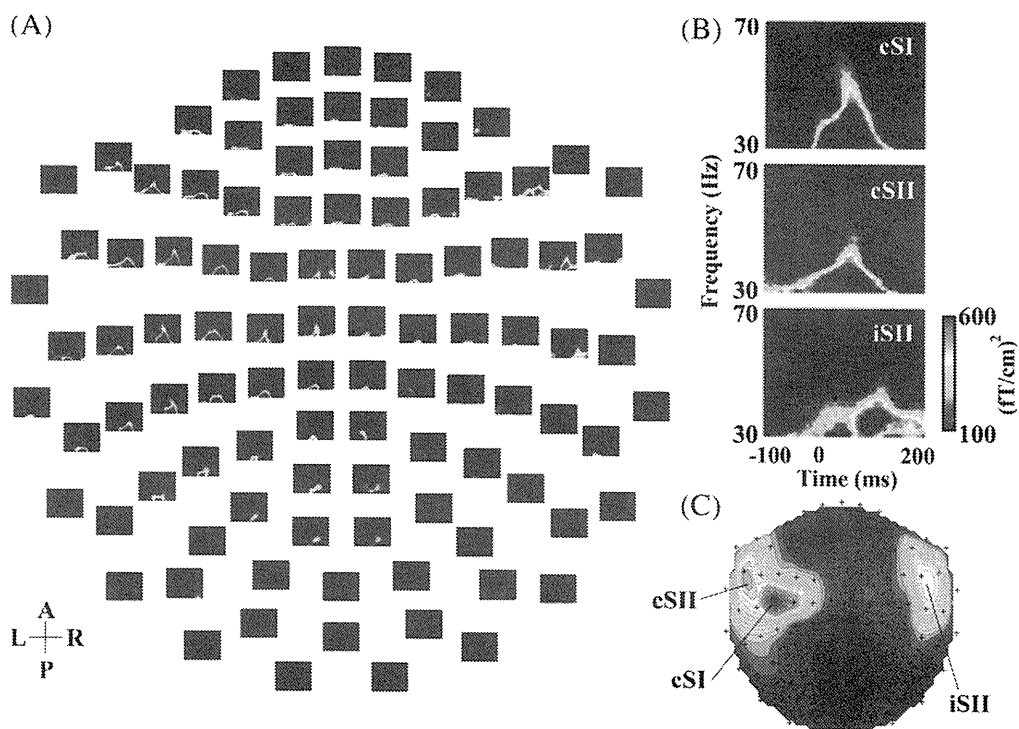
Fig. 6. (A) Temporal-frequency analysis for all gradiometer sensors in a representative MS patient. (B) Induced gamma activities recorded by the sensors showing the SI and SII activities. In contrast to normal subjects, the absolute power of the high-frequency gamma activities (50–70 Hz) is relatively reduced in cSI. (C) Topography of the induced gamma activities around the SI and SII areas.
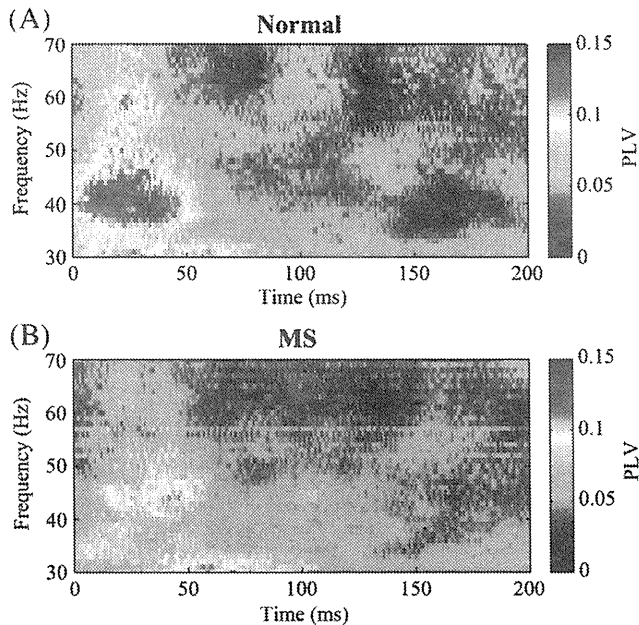
Fig. 7. Analysis of PLVs between cSI and cSII. (A) The grand average of PLVs in normal subjects shows increased PLVs in the entire gamma-frequency band (30–70 Hz). The high PLVs in the high-frequency gamma-band (50–70 Hz) are observed in the earlier latencies (mostly in the post-stimulus period of 20–50 ms), whereas those in the low-frequency gamma-band (30–40 Hz) last up to 100 ms. There are also some phase-locking activities of various frequencies during the later post-stimulus period (>100 ms). (B) In MS patients, decreased PLVs are noted in the entire frequency range.

of cSII started at around 20 ms after electrical stimulation of the median nerve, consistent with the latency of the direct thalamocortical conduction to SII. Likewise, short-latency responses in SII were reported by a study with direct cortical recording (Barba et al., 2002), which demonstrated that SEPs in SII could be generated at around 30 ms after the median nerve stimulation. Furthermore, transcranial magnetic stimulation delivered at the SII area at about 20 ms after electrical stimulation of the median nerve specifically caused facilitatory effect on motor reaction time (Raij et al., 2008), which proposed the presence of the direct thalamocortical pathway to SII. Although we could not record the early-latency evoked responses in SII, our results revealed a nonlinear relationship between the evoked responses in SI and SII. There was no significant correlation between the latencies of N20m and cSII both in normal subjects and MS patients. Moreover, analysis of SEFs showed no significant differences in the latencies and amplitudes of SII responses despite the prolonged latencies and decreased amplitudes of cSI deflections in MS patients. Thus, it is plausible that the early-latency gamma oscillations in SII, as reflected by the increased PLVs, might be partly mediated by the direct thalamocortical input to SII.

We demonstrated the decrease in PLVs between SI and SII in MS patients compared with normal control subjects. The temporal-frequency analysis demonstrated the preserved low-frequency gamma activities (30–40 Hz) in MS patients, whereas the phase synchronization was significantly impaired in the corresponding frequency range. We also found that the PLVs between cSI and cSII were reduced in the high-frequency gamma-band (50–70 Hz), while the power of the high-gamma activities was relatively decreased. One may argue that the decreased PLVs in the high-frequency gamma-band may be attributable to the reduced power of the activity in MS patients. However, PLV is theoretically independent of the power fluctuations (Lachaux et al., 1999). Because subcortical U-fiber lesions and periventricular white matter lesions in MS patients may frequently involve the intra- and interhemispheric associative pathways, the lesion load might significantly contribute to the decreased

neuronal synchronization within the somatosensory cortical network. In accord with this view, the significance of such altered functional connectivity in MS patients was reported by some studies (Leocani et al., 2000; Cover et al., 2006; Arrondo et al., 2009), demonstrating disturbed neuronal synchrony in various frequency bands. The impaired interhemispheric functional connectivity in MS was also suggested by the non-correlation between the cSII and iSII latencies in the patient group. Although the assessment of intracortical connectivity within SI in MS patients has been performed by a recent MEG study using a synchronization index for the gamma-band activity (Tecchio et al., 2008), it is notable that this is the first MEG study to demonstrate impaired functional connectivity between SI and SII in MS.

Our study also raises a question regarding the general assumption that cSII and iSII are activated sequentially via the transcallosal fibers. We observed no significant difference in the latencies and amplitudes of iSII between the healthy subjects and MS patients, despite the altered cSI activity and the impairment of functional connectivity between cSII and iSII in the latter group. Our findings suggest that the functional disconnection of the bilateral somatosensory cortices does not have a significant impact on iSII activity. Similarly, a previous MEG study performed in patients with ischemic stroke lesions showed preserved responses of iSII, despite the diminished responses of cSI and cSII (Forss et al., 1999). These observations suggest that iSII receives direct input from the thalamus, and thus, the responsiveness of iSII is relatively independent of the activities of the contralateral somatosensory cortices.

The multifocality of the lesions in MS may be a methodological reservation of this study. The effect of individual lesions could not be simply weighed due to dissemination of the lesions in the CNS. In addition, we observed no significant changes in the evoked responses of SII despite the impaired SI response in MS. One may argue that thalamocortical inputs can be reduced both in SI and SII and that the SII activities could also be affected. Since our patients showed only mild disability, patients with more severe disability may reveal different characteristics on the SII responses. Alternatively, given that
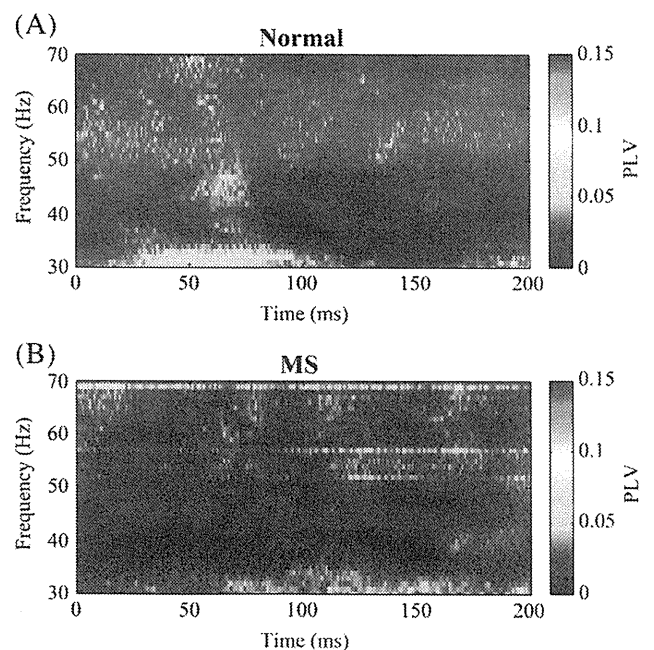
Fig. 8. Analysis of PLVs between cSII and iSII. (A) The grand average of PLVs in normal subjects shows significantly increased PLVs in the low-frequency gamma-band (30–40 Hz), which occurs between 30 and 100 ms. (B) Such an increase in PLVs is barely noticeable in MS patients.

SI receives input exclusively from the VPL and SII receives inputs from the multiple nuclei in the thalamus, it seems convincing that there exists a nonlinear relationship between the SI and SII responses. In accord with our assumption, an fMRI study demonstrated that patients with a solitary infarction of the VPL showed preserved activity of SII despite the reduced activation of SI (Taskin et al., 2006).

In conclusion, the analysis of PLVs demonstrated early neuronal synchronization between SI and SII. The decrease of PLVs in MS validated the significance of increased PLVs in healthy subjects. The current study provides evidence for the gamma-band synchrony in the early-stage human somatosensory processing.

Acknowledgment

Appendix A. Supplementary data

Supplementary data associated with this article can be found, in the online version, at doi:10.1016/j.neuroimage.2010.02.001.

References

Arrondo, G., Alegre, M., Sepulcre, J., Iriarte, J., Artieda, J., Villoslada, P., 2009. Abnormalities in brain synchronization are correlated with cognitive impairment in multiple sclerosis. Mult. Scler. 15, 509–516.

Balzamo, E., Marquis, P., Chauvel, P., Régis, J., 2004. Short-latency components of evoked potentials to median nerve stimulation recorded by intracerebral electrodes in the human pre- and postcentral areas. Clin. Neurophysiol. 115, 1616–1623.

Barba, C., Frot, M., Mauguière, F., 2002. Early secondary somatosensory area (SII) SEPs. Data from intracerebral recordings in humans. Clin. Neurophysiol. 113, 1778–1786.

Barkhof, F., Filippi, M., Miller, D.H., Scheltens, P., Campi, A., Polman, C.H., Comi, G., Ader, H.J., Losseff, N., Valk, J., 1997. Comparison of MRI criteria at first presentation to predict conversion to clinically definite multiple sclerosis. Brain 120, 2059–2069.

Bauer, M., Oostenveld, R., Peeters, M., Fries, P., 2006. Tactile spatial attention enhances gamma-band activity in somatosensory cortex and reduces low-frequency activity in parieto-occipital areas. J. Neurosci. 26, 490–501.

Buschman, T.J., Miller, E.K., 2007. Top-down versus bottom-up control of attention in the prefrontal and posterior parietal cortices. Science 315, 1860–1862.

Buzsáki, G., Draguhn, A., 2004. Neuronal oscillations in cortical networks. Science 304, 1926–1929.

Calabrese, P., Penner, I.K., 2007. Cognitive dysfunctions in multiple sclerosis—a "multiple disconnection syndrome"? J. Neurol. 254 (Suppl. 2), II18–II21.

Cover, K.S., Vrenken, H., Geurts, J.J., van Oosten, B.W., Jelles, B., Polman, C.H., Stam, C.J., van Dijk, B.W., 2006. Multiple sclerosis patients show a highly significant decrease in alpha band interhemispheric synchronization measured using MEG. Neuroimage 29, 783–788.

Dineen, R.A., Vilisaar, J., Hlinka, J., Bradshaw, C.M., Morgan, P.S., Constantinescu, C.S., Auer, D.P., 2009. Disconnection as a mechanism for cognitive dysfunction in multiple sclerosis. Brain 132, 239–249.

Engel, A.K., Singer, W., 2001. Temporal binding and the neural correlates of sensory awareness. Trends Cogn. Sci. 5, 16–25.

Engel, A.K., Fries, P., Singer, W., 2001. Dynamic predictions: oscillations and synchrony in top-down processing. Nat. Rev. Neurosci. 2, 704–716.

Forss, N., Hari, R., Salmelin, R., Ahonen, A., Hämäläinen, M., Kajola, M., Knuutila, J., Simola, J., 1994. Activation of the human posterior parietal cortex by median nerve stimulation. Exp. Brain Res. 99, 309–315.

Forss, N., Merlet, I., Vanni, S., Hämäläinen, M., Mauguière, F., Hari, R., 1996. Activation of human mesial cortex during somatosensory target detection task. Brain Res. 734, 229–235.

Forss, N., Hietanen, M., Salonen, O., Hari, R., 1999. Modified activation of somatosensory cortical network in patients with right-hemisphere stroke. Brain 122, 1889–1899.

Friedman, D.P., Murray, E.A., 1986. Thalamic connectivity of the second somatosensory area and neighboring somatosensory fields of the lateral sulcus of the macaque. J. Comp. Neurol. 252, 348–373.

Frot, M., Mauguière, F., 1999. Timing and spatial distribution of somatosensory responses recorded in the upper bank of the sylvian fissure (SII area) in humans. Cereb. Cortex 9, 854–863.

He, Y., Dagher, A., Chen, Z., Charil, A., Zijdenbos, A., Worsley, K., Evans, A., 2009. Impaired small-world efficiency in structural cortical networks in multiple sclerosis associated with white matter lesion load. Brain 132, 3366–3379.

Huttunen, J., Komssi, S., Lauronen, L., 2006. Spatial dynamics of population activities at S1 after median and ulnar nerve stimulation revisited: an MEG study. Neuroimage 32, 1024–1031.

Inui, K., Wang, X., Tamura, Y., Kaneoke, Y., Kakigi, R., 2004. Serial processing in the human somatosensory system. Cereb. Cortex 14, 851–857.

Iwamura, Y., 1998. Hierarchical somatosensory processing. Curr. Opin. Neurobiol. 8, 522–528.

Kakigi, R., 1994. Somatosensory evoked magnetic fields following median nerve stimulation. Neurosci. Res. 20, 165–174.

Karhu, J., Tesche, C.D., 1999. Simultaneous early processing of sensory input in human primary (SI) and secondary (SII) somatosensory cortices. J. Neurophysiol. 81, 2017–2025.

Kida, T., Wasaka, T., Inui, K., Akatsuka, K., Nakata, H., Kakigi, R., 2006. Centrifugal regulation of human cortical responses to a task-relevant somatosensory signal triggering voluntary movement. Neuroimage 32, 1355–1364.

Knight, R.T., 2007. Neuroscience. Neural networks debunk phrenology. Science 316, 1578–1579.

Krubitzer, L.A., Kaas, J.H., 1992. The somatosensory thalamus of monkeys: cortical connections and a redefinition of nuclei in marmosets. J. Comp. Neurol. 319, 123–140.

Kurtzke, J.F., 1983. Rating neurologic impairment in multiple sclerosis: an expanded disability status scale (EDSS). Neurology 33, 1444–1452.

Lachaux, J.P., Rodriguez, E., Martinerie, J., Varela, F.J., 1999. Measuring phase synchrony in brain signals. Hum. Brain Mapp. 8, 194–208.

Leocani, L., Locatelli, T., Martinelli, V., Rovaris, M., Falautano, M., Filippi, M., Magnani, G., Comi, G., 2000. Electroencephalographic coherence analysis in multiple sclerosis: correlation with clinical, neuropsychological, and MRI findings. J. Neurol. Neurosurg. Psychiatry 69, 192–198.

Lin, Y.Y., Forss, N., 2002. Functional characterization of human second somatosensory cortex by magnetoencephalography. Behav. Brain Res. 135, 141–145.

Matsuoka, T., Matsushita, T., Kawano, Y., Osoegawa, M., Ochi, H., Ishizu, T., Minohara, M., Kikuchi, H., Mihara, F., Ohyagi, Y., Kira, J., 2007. Heterogeneity of aquaporin-4 autoimmunity and spinal cord lesions in multiple sclerosis in Japanese. Brain 130, 1206–1223.

Mauguière, F., Merlet, I., Forss, N., Vanni, S., Jousmäki, V., Adeleine, P., Hari, R., 1997. Activation of a distributed somatosensory cortical network in the human brain. A dipole modelling study of magnetic fields evoked by median nerve stimulation. Part I: location and activation timing of SEF sources. Electroencephalogr. Clin. Neurophysiol. 104, 281–289.

Palva, S., Linkenkaer-Hansen, K., Näätänen, R., Palva, J.M., 2005. Early neural correlates of conscious somatosensory perception. J. Neurosci. 25, 5248–5258.

Polman, C.H., Reingold, S.C., Edan, G., Filippi, M., Hartung, H.P., Kappos, L., Lublin, F.D., Metz, L.M., McFarland, H.F., O'Connor, P.W., Sandberg-Wollheim, M., Thompson, A.J., Weinshenker, B.G., Wolinsky, J.S., 2005. Diagnostic criteria for multiple sclerosis: 2005 revisions to the "McDonald Criteria". Ann. Neurol. 58, 840–846.

Pons, T.P., Garraghty, P.E., Friedman, D.P., Mishkin, M., 1987. Physiological evidence for serial processing in somatosensory cortex. Science 237, 417–420.

Raij, T., Karhu, J., Kicić, D., Lioumis, P., Julkunen, P., Lin, F.H., Ahveninen, J., Ilmoniemi, R.J., Mäkelä, J.P., Hämäläinen, M., Rosen, B.R., Belliveau, J.W., 2008. Parallel input makes the brain run faster. Neuroimage 40, 1792–1797.

Saalmann, Y.B., Pigarev, I.N., Vidyasagar, T.R., 2007. Neural mechanisms of visual attention: how top-down feedback highlights relevant locations. Science 316, 1612–1615.

Simões, C., Jensen, O., Parkkonen, L., Hari, R., 2003. Phase locking between human primary and secondary somatosensory cortices. Proc. Natl. Acad. Sci. U. S. A. 100, 2691–2694.

Stevens, R.T., London, S.M., Apkarian, A.V., 1993. Spinothalamocortical projections to the secondary somatosensory cortex (SII) in squirrel monkey. Brain Res. 631, 241–246.

Tallon-Baudry, C., Bertrand, O., 1999. Oscillatory gamma activity in humans and its role in object representation. Trends Cogn. Sci. 3, 151–162.

Tallon-Baudry, C., Bertrand, O., Delpuech, C., Permier, J., 1997. Oscillatory gamma-band (30–70 Hz) activity induced by a visual search task in humans. J. Neurosci. 17, 722–734.

Taskin, B., Jungehulsing, G.J., Ruben, J., Brunecker, P., Krause, T., Blankenburg, F., Villringer, A., 2006. Preserved responsiveness of secondary somatosensory cortex in patients with thalamic stroke. Cereb. Cortex 16, 1431–1439.

Taulu, S., Simola, J., 2006. Spatiotemporal signal space separation method for rejecting nearby interference in MEG measurements. Phys. Med. Biol. 51, 1759–1768.

Tecchio, F., Zito, G., Zappasodi, F., Dell' Acqua, M.L., Landi, D., Nardo, D., Lupoi, D., Rossini, P.M., Filippi, M.M., 2008. Intra-cortical connectivity in multiple sclerosis: a neurophysiological approach. Brain 131, 1783–1792.

Wegner, K., Forss, N., Salenius, S., 2000. Characteristics of the human contra- versus ipsilateral SII cortex. Clin. Neurophysiol. 111, 894–900.

Wikström, H., Huttunen, J., Korvenoja, A., Virtanen, J., Salonen, O., Aronen, H., Ilmoniemi, R.J., 1996. Effects of interstimulus interval on somatosensory evoked magnetic fields (SEFs): a hypothesis concerning SEF generation at the primary sensorimotor cortex. Electroencephalogr. Clin. Neurophysiol. 100, 479–487.

Womelsdorf, T., Fries, P., Mitra, P.P., Desimone, R., 2006. Gamma-band synchronization in visual cortex predicts speed of change detection. Nature 439, 733–736.

Womelsdorf, T., Schoffelen, J.M., Oostenveld, R., Singer, W., Desimone, R., Engel, A.K., Fries, P., 2007. Modulation of neuronal interactions through neuronal synchronization. Science 316, 1609–1612.

Zhang, H.Q., Murray, G.M., Turman, A.B., Mackie, P.D., Coleman, G.T., Rowe, M.J., 1996. Parallel processing in cerebral cortex of the marmoset monkey: effect of reversible SI inactivation on tactile responses in SII. J. Neurophysiol. 76, 3633–3655.

Zhang, H.Q., Zachariah, M.K., Coleman, G.T., Rowe, M.J., 2001. Hierarchical equivalence of somatosensory areas I and II for tactile processing in the cerebral cortex of the marmoset monkey. J. Neurophysiol. 85, 1823–1835.

Spatiotemporal signatures of an abnormal auditory system in stuttering

Yoshikazu Kikuchi [a,b], Katsuya Ogata [b,*], Toshirou Umesaki [a], Takashi Yoshiura [c], Masamutsu Kenjo [f], Yoji Hirano [d], Tsuyoshi Okamoto [e], Shizuo Komune [a], Shozo Tobimatsu [b]

[a] Department of Otolaryngology, Faculty of Medicine, Graduate School of Medical Sciences, Kyushu University, Fukuoka, Japan
[b] Department of Clinical Neurophysiology, Faculty of Medicine, Graduate School of Medical Sciences, Kyushu University, Fukuoka, Japan
[c] Department of Clinical Radiology, Faculty of Medicine, Graduate School of Medical Sciences, Kyushu University, Fukuoka, Japan
[d] Department of Neuropsychiatry, Faculty of Medicine, Graduate School of Medical Sciences, Kyushu University, Fukuoka, Japan
[e] Department of Digital Medicine Initiative, Faculty of Medicine, Graduate School of Medical Sciences, Kyushu University, Fukuoka, Japan
[f] Department of Special Education, Fukuoka University of Education, Fukuoka, Japan

ARTICLE INFO

ABSTRACT

People who stutter (PWS) can reduce their stuttering rates under masking noise and altered auditory feedback; such a response can be attributed to altered auditory input, which suggests that abnormal speech processing in PWS results from abnormal processing of auditory input. However, the details of this abnormal processing of basic auditory information remain unclear. In order to characterize such abnormalities, we examined the functional and structural changes in the auditory cortices of PWS by using a 306-channel magnetoencephalography system to assess auditory sensory gating (P50m suppression) and tonotopic organization. Additionally, we employed voxel-based morphometry to compare cortical gray matter (GM) volumes on structural MR images. PWS exhibited impaired left auditory sensory gating. The tonotopic organization in the right hemisphere of PWS is expanded compared with that of the controls. Furthermore, PWS showed a significant increase in the GM volume of the right superior temporal gyrus, consistent with the right tonotopic expansion. Accordingly, we suggest that PWS have impaired left auditory sensory gating during basic auditory input processing and that some error signals in the auditory cortex could result in abnormal speech processing. Functional and structural reorganization of the right auditory cortex appears to be a compensatory mechanism for impaired left auditory cortex function in PWS.

Introduction

Stuttering is a developmental disorder that affects speech fluency. This disorder is observed in 5% of children aged between 2 and 4 years (Månsson, 2000). The mechanism of stuttering is still a matter of debate. People who stutter (PWS) decrease their stuttering rates temporarily under masking noise and altered auditory feedback, which is not only because of the resulting slower speech rate but also because of altered auditory input (Altrows and Bryden, 1977; Kalinowski et al., 1993; Lincoln et al., 2006; Hampton and Weber-Fox, 2008). This suggests that auditory input processing could be different in PWS compared with

non-stuttering subjects. Postma and Kolk (1992) proposed "auditory feedback defect theories in PWS," in which PWS have deviant error monitoring of speech production, namely, PWS detect errors more than people who do not stutter. Postma and Kolk (1993) and Postma (2000) also proposed "the covert repair hypothesis," in which stuttering derives from the need to repeatedly repair errors before and after speech motor movement. Thereafter, Max et al. (2004) proposed "internal models and feedback-biased motor control theory". In this hypothesis, a motor plan is constructed and executed by a feedforward controller, and execution is adjusted by a feedback controller that integrates in real time both afferent (auditory) and efferent (motor) signals. They speculated that stuttering resulted from a mismatch between predicted (feedforward) and actual (feedback) consequences of the executed movements. Overall, stuttering could be related to impaired auditory–motor integration.

Fox et al. (1996) performed neuroimaging studies and reported that stuttering is a disorder of integration within the speech system and not of a single area. Subsequently, stutter-typical networks are not only involved in an extended right-hemispheric network, including the frontal operculum, the temporo-parietal junction, and the dorsolateral prefrontal cortex (Kell et al., 2009), but also in the impaired left-hemispheric network, including the arcuate fasciculus

(Sommer et al., 2002; Chang et al., 2008; Watkins et al., 2008; Cykowski et al., 2010), which connects temporal regions with frontal speech motor-planning (including Broca's area) and motor regions, as well as the striato-thalamico-cortico-striatal loop, which has important connections to the auditory regions (Giraud et al., 2008). Additionally, Chang et al. (2008) identified bilaterally abnormal fractional anisotropy in the corticospinal/corticobulbar tract (which is involved in speech motor control) and in a posterior-lateral region underlying the supramarginal gyrus (rostral portion of the inferior parietal lobe that is connected to the classic frontotemporal language areas) in stuttering children. Watkins et al. (2008) also found disturbed integrity of the white matter underlying the functional underactive areas in the ventral premotor cortex (a connection with posterior-superior temporal and inferior parietal cortex), which provides a substrate for the integration of articulatory planning and sensory feedback. Fluency-shaping therapies reduce right hemispheric over-activation, normalize basal ganglia activity and reactivate left-hemispheric cortex (De Nil et al., 2003; Neumann et al., 2005; Giraud et al., 2008; Kell et al., 2009). Taken together, abnormal auditory–motor integration can be the neural basis of stuttering.

Auditory–motor integration has been investigated in 2 magnetoencephalographic (MEG) studies (Salmelin et al., 1998; Beal et al., 2010). Salmelin et al. (1998) recorded auditory evoked magnetic fields to a single pure tone during the performance of 4 language-related tasks (reading silently, mouth movements only, reading aloud, and reading in chorus with another person). They found that the interhemispheric balance of the N100m responses of PWS was affected more severely by the tasks involving speech than by the 2 non-verbal tasks. Beal et al. (2010) reported the phenomenon of speech-induced suppression of the auditory N100m for vowel stimuli and showed that both the P50m and N100m were suppressed for word stimuli. They also revealed that the P50m and N100m latencies in PWS were significantly longer than those in the controls, which suggested that the timing of cortical auditory processing in PWS was slower than that in controls under various stimuli. These findings support the altered auditory–motor integration in PWS.

Therefore, we hypothesized that PWS have an abnormal auditory–motor integration system. We tested our hypothesis by using auditory sensory gating that modulates auditory inputs and tonotopic organization that corresponds to auditory inputs. PWS do not have abnormal auditory inputs to brainstem responses (Decker et al., 1982; Newman et al., 1985; Stager, 1990). To validate our hypothesis, we conducted 3 experiments. First, we examined auditory sensory gating by MEG using a P50m (or P50 in EEG) suppression standard paradigm, as has been used in studies on schizophrenia and Alzheimer's disease (Adler et al., 1982; Jessen et al., 2001; Thoma et al., 2003; Hirano et al., 2010). We presented 2 successive click sounds to the subjects monaurally, and the lack of P50m suppression in response to the second sound suggested an inability to filter unnecessary auditory information. Second, we measured the most frequently used N100m in response to 3 tonal stimuli at 250, 1000, and 4000 Hz to elucidate the expansion of the tonotopic map (Pantev et al., 1998b; Naka et al., 1999). MEG has both high spatial and temporal resolution and can be used to evaluate the differences in tonotopic organization in both auditory cortices of PWS and controls. Third, we performed three-dimensional voxel-based morphometry (VBM) to assess structural changes in the auditory cortex. Using the results of these studies, we have provided electrophysiological and structural evidence for abnormal auditory processing in PWS.

Methods

Experiment 1: Auditory sensory gating

Subjects

Seventeen men who stutter (mean age, 30.2 ± 5.7 years; range, 21–41 years) and 18 control male subjects (mean age, 30.6 ±

6.2 years; range, 22–43 years) participated in the present study. PWS were recruited from a self-help group as volunteers and were diagnosed as having developmental stuttering according to DSM-IV (Diagnostic and Statistical Manual of Mental Disorders-IV). All subjects gave their written informed consent for participation in the study, and the study was approved by the Ethics Committee of Kyushu University. None of the participants had a history of otological or neurological disorders, and all were right-handed according to the Edinburgh Handedness Inventory (Oldfield, 1971). Unfortunately, we were unable to enroll the same participants across all experiments.

The severity of stuttering was assessed by a speech-language-hearing therapist as the percentage of stuttered syllables of at least 300 analyzable syllables averaged over 3 different speaking contexts (reading a short story, describing pictures, and asking questions) and rated as 8.4% (range, 0.8%–36.7%) for PWS and 0.22% (range, 0%–0.55%) for the control group. We excluded 1 subject because of a low dysfluency of less than 1% (Jones et al., 2005; Kell et al., 2009). The stuttered syllables included only the instances of unambiguous stuttering (Jones et al., 2000) and incorporated syllable repetitions and audible and inaudible sound prolongations (Conture, 2001), except normal dysfluencies such as interjections, whole-word repetitions, revisions, and phrase-repetitions.

Stimulus setting

Auditory stimuli were 3-ms monaural clicks presented in pairs with a 500-ms interstimulus interval (ISI) and an intertrial interval that randomly varied between 8 and 12 s (Thoma et al., 2003). The hearing threshold was determined for each subject, and the stimuli were delivered at an intensity of 30 dB above the threshold so as not to induce cross-hearing. The subjects received the stimuli from a Tone Burst Generator (Kyushu Keisokuki, Japan) passed through a plastic tube (length, 6 m; inner diameter, 8 mm) into sponge ear pieces fitted in the subjects' ears. The subjects were in supine position.

MEG recording

Auditory evoked magnetic fields were measured using a whole-head 306-channel biomagnetometer system (Elekta-Neuromag, Helsinki, Finland) in a quiet, magnetically shielded room. The detector array comprised 102 identical triple sensor elements, with each sensor element comprising 2 orthogonally oriented planar-type gradiometers and 1 magnetometer. Planar gradiometers pick up the strongest signals just above the local current, and consequently, the locations of the sensors detecting the strongest signals could be readily used as the first guesses of the activated brain areas (Hämäläinen et al., 1993). Prior to the recording, four head position indicator (HPI) coils were attached to the scalp, and a 3D digitizer was used to measure anatomical landmarks of the head with respect to the HPI coils. During data acquisition, the HPI coils were continuously active and the head position was continuously measured. The magnetic responses were digitally sampled at a rate of 1000 Hz. In order to keep subjects alert and to prevent them from paying attention to the auditory stimuli, we instructed them to watch a silent cartoon movie during the recordings (Thoma et al., 2008; Weisser et al., 2001).

After a recording, the movement compensation realized by the temporal extension signal space separation (MC-tSSS) with Maxfilter 2.0 software (Elekta Neuromag®) was applied off-line to the recorded raw data to reduce artifact signals arising from outside the sensor array and to correct the head position as well as the associated movement-related artifacts (Taulu et al., 2004, 2005; Medvedovsky et al., 2007). Off-line averaging of the auditory event-related field (AEF) was performed using the MC-tSSS-reconstructed raw data, and 150 responses were averaged for each ear. A −100 to −10 ms baseline adjustment and a 5–55 Hz bandpass filter (Thoma et al., 2003; Lu et al., 2007) were then applied to the AEF. Of the 306 channels recorded, 70 channels, including the P50m signal

contralateral to the stimulus, were selected for analysis (Fig. 1A). We analyzed the AEFs contralateral to the stimulated ear, which are usually larger than the ipsilateral AEFs (Pantev et al., 1986). The peak latencies and amplitudes of the AEFs were determined by root mean square (RMS) waveforms reconstructed from the gradiometers. A single equivalent current dipole (ECD) was calculated, yielding 3-dimensional coordinates of the P50m responses. The origin of this coordinate system was set at the midpoint of the medial–lateral axis (x axis), which joined the center points of the entrance to the external acoustic meatus of both sides (positive toward the right ear). The anterior–posterior axis (y axis) was oriented from the origin to the nasion (positive toward the nasion) and the inferior–superior axis (z axis) was perpendicular to the x–y plane (positive toward the vertex). The locations of the ECDs were standardized with their origins and radii. For estimating the ECD of P50m, 10-ms data across the time point showing the maximal amplitude of P50m were selected from the RMS waveforms, and the ECDs with the largest dipole moment over the period were selected. The calculated ECD strengths and locations were accepted for further analysis when they satisfied the following criteria: (1) a P50m peak latency between 20 and 70 ms, and (2) a goodness-of-fit greater than 75% (Hirano et al., 2008, 2010; Thoma et al., 2003). P50m suppression was expressed as a ratio of the P50m dipole moment evoked by S2 (Q2) to that evoked by S1 (Q1). We used Q2/Q1 as a measure of the disinhibition of auditory sensory gating (Thoma et al., 2003; Lu et al., 2007).

Statistical analysis

In order to analyze the P50m Q2/Q1, latency, and locations, we performed repeated-measures multivariate analysis of variance (MANOVA) with hemisphere (left vs. right) as the within-subject factor and group (PWS vs. controls) as the between-subject factor using SPSS 11.5. Post-hoc analyses were conducted using multiple comparisons with Bonferroni correction. The significance level was set at 0.05. The association between Q2/Q1 and stuttering rate was evaluated using Pearson's correlation coefficient.

Experiment 2: Tonotopic organization

Subjects

Sixteen men who stutter (mean age, 30 ± 5.8 years; range, 21–41 years) and 16 control male subjects (mean age, 30.8 ± 6.4 years; range, 22–43 years) participated in this experiment. Fourteen PWS and 13 controls who participated in experiment 1 also participated in this experiment. The severity of stuttering was rated as 8.4% (range, 0.8% to 36.7%) for PWS and 0.22% (range, 0% to 0.55%) for the control group. We excluded 1 subject because of low disfluency. The other conditions were the same as those described for experiment 1.

Stimulus delivery

Each auditory tone-burst stimulus of 250, 1000, and 4000 Hz (300-ms duration, with a 10-ms rise and 20-ms fall) was monaurally
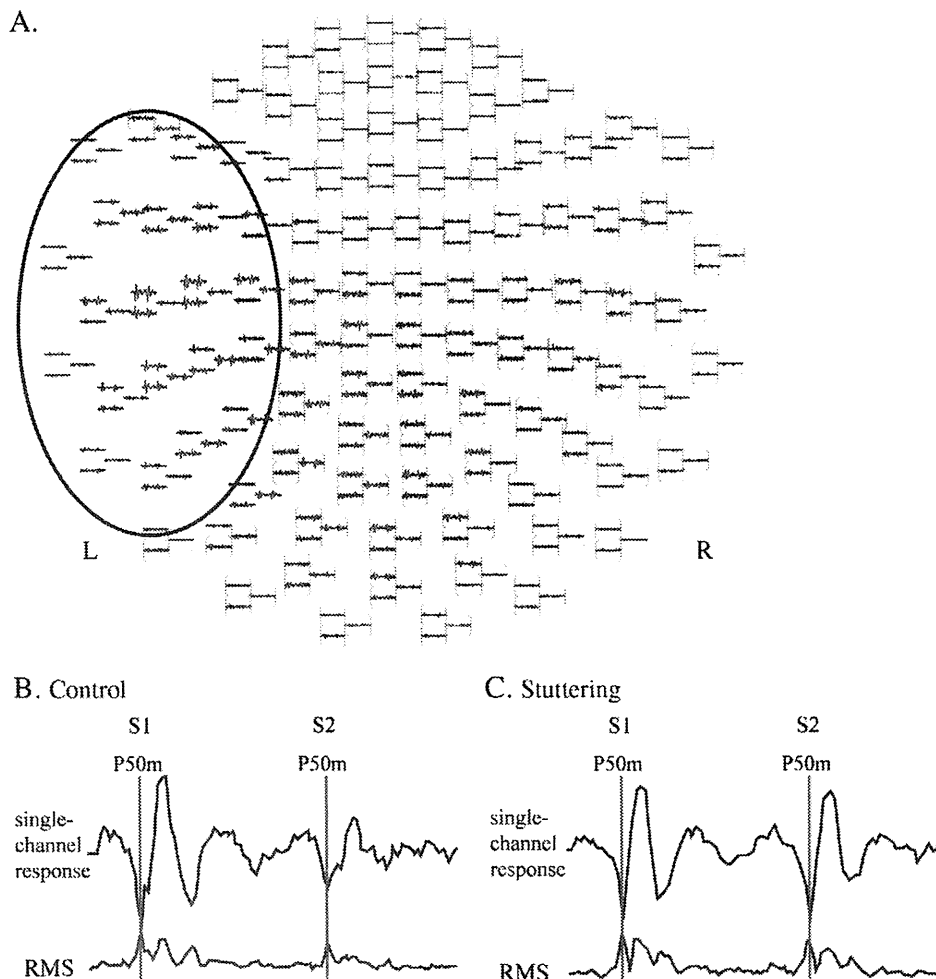
Fig. 1. The source of the P50m response estimated by MEG. Seventy channels around the P50m peak in the left hemisphere (encircled) were used to fit a single dipole source (A). Single-channel response and root mean squares (RMS) over the selected channels in a representative control subject. The response to S2 is apparently smaller than that to S1 (B). The response to S2 is only slightly smaller than that to S1 in a representative stuttering subject (C).

presented more than 128 times in a random order. The ISI was distributed between 2.5 and 3.5 s. The peak stimulus intensity was set at 30 dB above the hearing threshold.

MEG recording

The averaged evoked fields were referred to a baseline from −100 to −10 ms and filtered from 1 to 20 Hz (Pantev et al., 1995; Elbert et al., 2002; Rojas et al., 2002). The dipole moment, location, and latency of the N100m source were determined in a manner similar to that described for experiment 1. The calculated values were accepted for further analysis if they satisfied the following criteria: (1) an N100m latency between 80 and 160 ms of the RMS peak; (2) a goodness-of-fit value of the ECD greater than 85%; and (3) a confidence volume less than 100 mm^3 (Elbert et al., 2002; Rojas et al., 2002).

Statistical analysis

The N100m source amplitudes, latency, and locations were analyzed using a repeated-measures MANOVA with a between-subject factor of group and within-subject factors of hemisphere and frequency (250, 1000, and 4000 Hz). Post-hoc analyses were performed using multiple comparisons with Bonferroni correction. In order to examine the expansion of the tonotopic map, we fitted linear regression lines for each direction of the x (medial–lateral) and y (anterior–posterior) axes and calculated the regression coefficient. When N100m dipole locations are plotted against the logarithm of frequency, they can be represented by a straight line (Pantev et al., 1995, 1998a). Thereafter, we compared the regression coefficient by using a repeated-measures MANOVA with a between-subject factor of group and a within-subject factor of hemisphere. The association between tonotopic map expansion and stuttering rate was evaluated using Pearson's correlation coefficient.

Experiment 3: Voxel-based morphometry

Subjects

Fifteen men who stutter (mean age, 30 ± 5.8 years; range, 21–41 years) and 15 control male subjects (mean age, 30.8 ± 6.4 years; range, 22–43 years) participated in this experiment. Thirteen PWS who participated in both experiments 1 and 2 also participated in this study. The other conditions were the same as those described for experiment 2.

Image processing

Three-dimensional volumetric T1-weighted MR images were obtained using a 1.5-T MRI scanner (Achieva Nova Dual; Philips Medical Systems, Best, Netherlands). We used a field-echo three-dimensional sagittal pulse sequence with the following parameters: TR = 25 ms, TE = 4.6 ms, field of view = 230 mm, flip angle = 30°, matrix = 240 × 240, and slice thickness = 1 mm. The images were obtained in the sagittal plane and were then reconstructed into 1-mm-thick contiguous transverse images.

Analysis

VBM was performed using the toolbox Diffeomorphic Anatomical Registration Through Exponential Lie algebra (DARTEL) of SPM8 (Wellcome Department of Imaging Neuroscience, London, UK). DARTEL is a suite of tools for achieving more accurate intersubject registration of brain images (Ashburner, 2007). DARTEL preprocessing includes 3 steps. The first step involves generating the roughly aligned gray matter (GM) images of the subjects by using "New Segment," which can be used with an East Asian template, and was found to be more robust than the "Unified Segmentation" of SPM8. The second step involves determining the nonlinear deformations for warping all the GM images by using "Run DARTEL (create Template)" so that they matched each other. The final step involves generating 8-mm smoothed and modulated normalized GM images with a voxel size of 1.5 × 1.5 × 1.5 mm by using "Normalise to MNI Space."

Group comparisons were conducted using a two-sample t test with an absolute threshold mask of 0.05. Whole brain data were analyzed using a height threshold of T = 3.26 (p < 0.001, uncorrected) because of small group sizes. Uncorrected VBM data were also adopted in the previous studies (Chang et al., 2008; Beal et al., 2007; Kell et al., 2009).

Results

Experiment 1: Auditory sensory gating

In both groups, 2 successive clicks evoked a well-defined P50m response in the hemisphere contralateral to the stimulated ear (Fig. 1). Fig. 1A shows the data from 70 channels around the sensor with a maximal amplitude of P50m in the left hemisphere. Figs. 1B and C show the representative waveforms of P50m in a normal control and a stuttering subject, respectively. The amplitude of S2-P50m was apparently smaller than that of S1-P50m in the control subjects; however, no such amplitude difference between S1-P50m and S2-P50m was evident in stuttering subjects.

Table 1 summarizes the dipole moments (Q1 and Q2), latency of S1-P50m and S2-P50m, and the Q2/Q1 ratio (mean ± SEM). MANOVA of the Q2/Q1 ratio revealed a significant group × hemisphere interaction [F(1, 31) = 4.209, p = 0.048]. As shown in Fig. 2A, the Q2/Q1 ratio for the left hemisphere was significantly smaller than that for the right hemisphere in the controls (p = 0.024). In contrast, there was no significant difference between hemispheres in PWS. The Q2/Q1 ratio for the left hemisphere in PWS was significantly larger than that in the controls (p = 0.014).

The right S1-P50m latency in PWS was significantly shorter than the left S1-P50m latency (p = 0.047); however, this was not the case for the controls. In each subject, P50m dipolar sources were located in the superior temporal gyrus (STG) close to Heschl's gyrus, and there were no significant differences in the source locations between the 2 groups. Moreover, there was no significant correlation between the Q2/Q1 ratio and stuttering rate or between the S1-P50m latencies and stuttering rate.

Experiment 2: Tonotopic organization

In both groups, an N100m response was clearly evoked by each tonal frequency in the hemisphere contralateral to the stimulated ear. Fig. 3A shows the data from 70 channels around the sensor with a maximal amplitude of N100m, and Figs. 3B and C show representative waveforms of N100m in a control and a stuttering subject, respectively. Fig. 4 shows tonotopic arrangements superimposed on individual MR images in representative subjects of both groups. Table 2 summarizes the ECD locations of N100m (mean ± SEM). Tonotopic organization was observed in x (medial–lateral) and y (anterior–posterior) coordinates in which higher frequencies were arranged medially and posteriorly. Regarding the y coordinate, there was a significant main effect of frequency [F(2, 24) = 22.7, p < 0.001] and hemisphere [F(1, 25) = 35.1, p < 0.001], which confirmed that there was a tonotopic organization with laterality. Although the main

Table 1
The mean latency (ms) and dipole moment (nAm) of S1 and S2 and the Q2/Q1 ratio of P50m.

	PWS		Controls	
	Left	Right	Left	Right
S1 Dipole moment (Q1)	15.3 ± 2.9	19 ± 2.4	15.6 ± 2.0	16.3 ± 1.9
S1 Latency	46.7 ± 2.0	42.6 ± 1.5	47.1 ± 1.1	44.3 ± 1.0
S2 Dipole moment (Q2)	12.9 ± 2.3	14.6 ± 1.9	9.8 ± 1.1	13 ± 1.5
S2 Latency	44.9 ± 1.8	43.5 ± 1.4	44.5 ± 1.4	45.1 ± 1.4
Q2/Q1	0.87 ± 0.08	0.81 ± 0.08	0.64 ± 0.04	0.86 ± 0.09

Values are expressed as mean ± SEM in this table and in Table 2.